Preliminary design of a high-altitude kite

A flexible membrane kite section at various angles of attack

In an earlier paper, titled *A flexible membrane kite section at high and low altitudes*, I examined a flexible membrane intended to represent a cross-section of a wing-shaped kite. The leading edge of the section was a round tube; the trailing edge of the nylon membrane was tied back by "trailing edge strings". In the earlier paper, I looked at the shape of this section when flying near sea level and at an altitude of 15,000 feet.

In this paper, I want to look more closely at the behaviour of this kind of thin membrane airfoil at different angles of attack.

I want to begin this study by changing slightly the chordwise dimensions of the section used in the earlier paper. In that paper, the membrane was based on a one meter width of rip stop nylon with a one centimeter hem sewn into both the fore and aft edges. The leading edge tube was a one-inch diameter thin-walled aluminum tube. The new section will keep both the nylon sheet and the aluminum tube. The ribs n the earlier paper were thin carbon fibre tubes. These tubes were one meter in length and were attached butt-end to the outside of the leading edge tube. Eight centimeters will now be cut off these tubes, so the ribs in the new section will be 92 centimeters long. The trailing edge strings in the earlier paper were ten centimeters long. They, too, will be shortened, but by slightly less than the amount by which the ribs will be shortened. The trailing edge strings will be shortened by seven centimeters, to a length of three centimeters. The camber of the new profile will be slightly greater than the one in the earlier paper. The following figure shows the key dimensions in the chordwise direction.

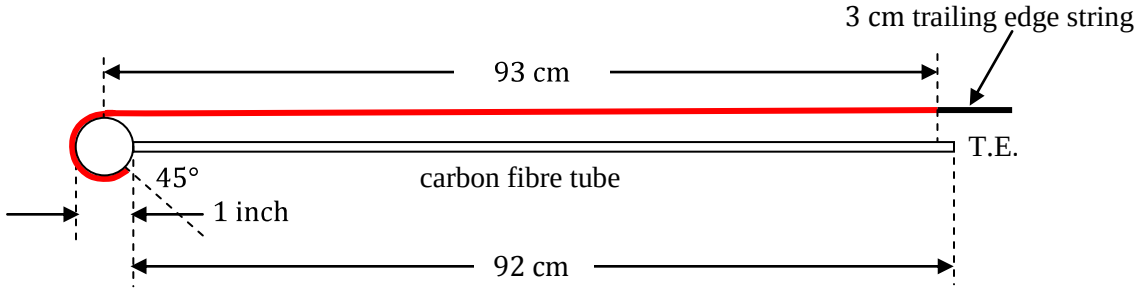

In this paper, we will simulate two flight conditions. Case #1 will be at sea level with a 10 mph wind speed. Case #2 will be at 15,000 feet with a 20 mph wind speed. Within each case, we will look at a range of angles of attack.

As in the earlier paper, the nylon membrane will be divided into 500 short segments of equal length. The discretization will include the entire width of the nylon, including the part which is wrapped against the leading edge tube. The VisualBasic program which calculates the shape of the free-flying segments for a given distribution of aerodynamic forces is the same one used in the earlier paper. The virtual wind tunnel used by OpenFoam is the same, too. All OpenFoam runs were continued until such time as all residuals were less than 10^{-5}. The overall procedure consists of iterations in which the forces and moments calculated by an OpenFoam simulation are used to re-calculate the shape of the membrane to be used in the next OpenFoam simulation. For each angle of attack sub-case examined in this paper, a total of five OpenFoam simulations were carried out.

Results for Case #1, at sea level in a 10 mph wind

The kite section was tested at angles of attack from 5° to 17°. Let me describe why angles of attack outside this range were not tested.

The OpenFoam simulation failed to converge when the angle of attack was 5°. The following figure shows the trajectory of the residuals during the second OpenFoam run at this angle of attack.

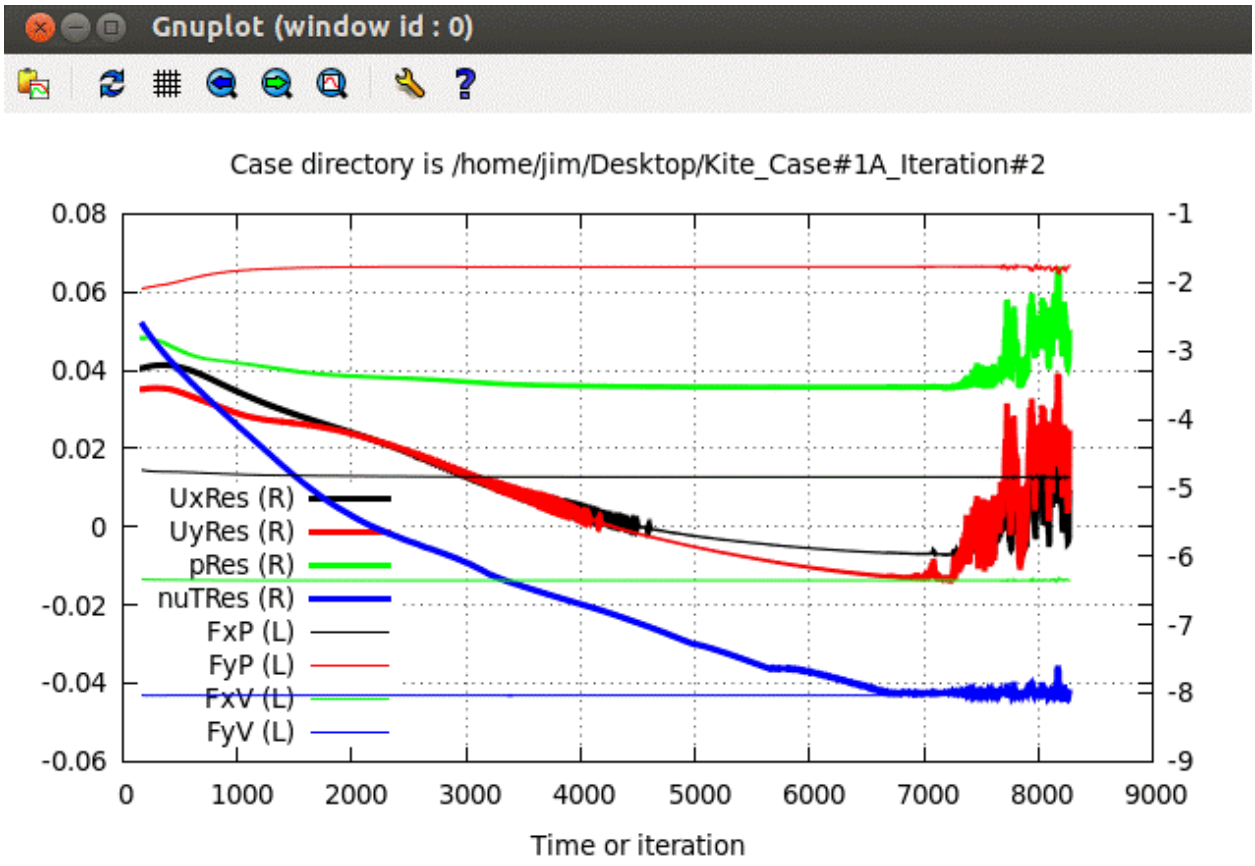

It is possible that a change in the parameters in OpenFoam's `/fvSolution` file would have led to convergence. What is important is that the parameters used for all the other angle of attack sub-cases did not result in convergence. For some reason, the pattern of airflow at this low an angle of attack was beginning to differ substantially from the pattern observed in other sub-cases. One expects intuitively that there is a minimum angle of attack at which the membrane will remain inflated. At too low an angle of attack, the membrane will begin to "luff" near the leading edge tube. It is enough for my purpose to treat the failure at a 5° angle of attack as the onset of luffing. I would not willingly fly a kite this close to trouble, as defined by possible deflation of the section.

Now, let's look at the other extreme, at high angles of attack. One expects intuitively that the airflow will begin to separate from the top surface of the membrane at high enough angles of attack. The following two pictures show the pattern of streamtracers around the section at angles of attack of 15° and 17°. At the former, the flow is starting to separate from the surface at about 70% of the chord. At a 17° angle of attack, the separation point has moved further forward, to about 50% of chord.

As the amount of separation increases, the benefits of streamlined airflow, being a higher lift-to-drag ratio, are increasingly lost. I would not willingly fly a kite which is this close to a stall.

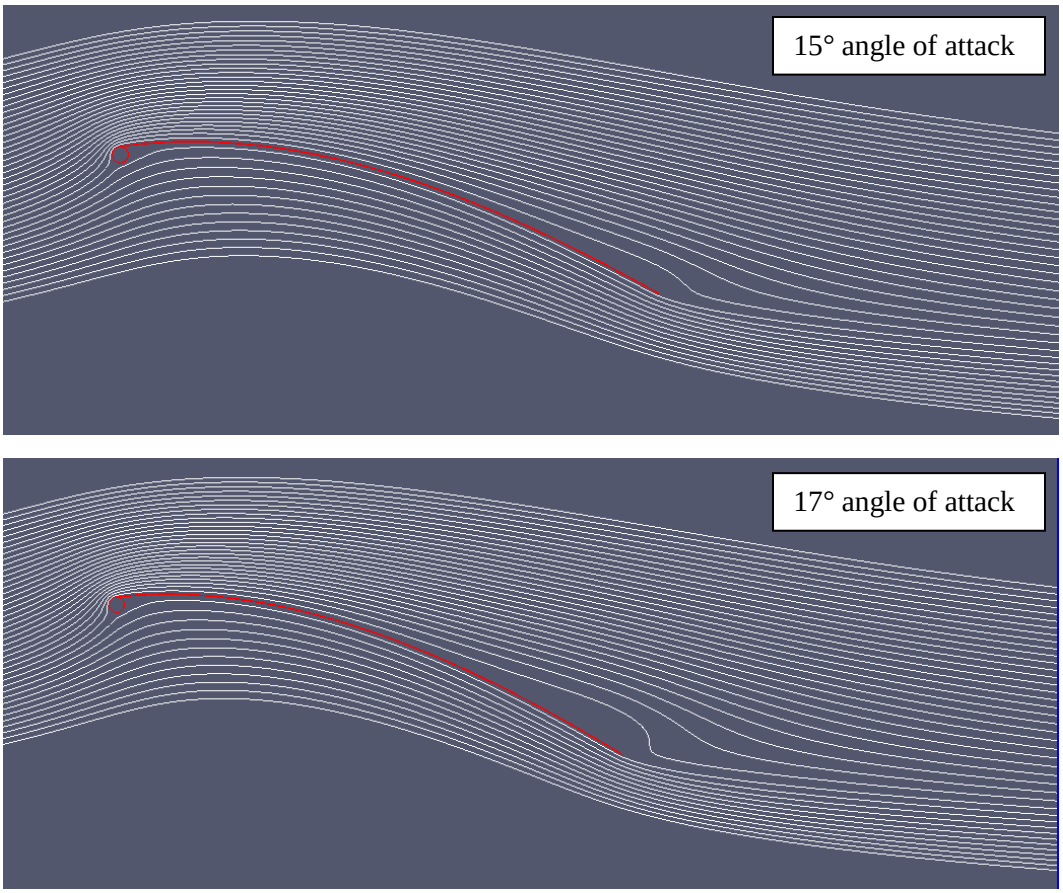

So, for Case #1, I will restrict my attention to the range of angles of attack from 6° to 17°. The following graph shows how the shape of the membrane changes with angle of attack. To generate this graph, the shapes of the membrane at all angles of attack were rotated to a common reference chord. I selected the shape at an 8° angle of attack to use as a reference shape. For each of the other angles of attack, I calculated the difference between the displacement from the reference chord (the vertical displacement) for the given angle of attack and the corresponding displacement at the 8° angle of attack. the vertical axis in the following graph is the difference in vertical displacement from the 8° reference shape.

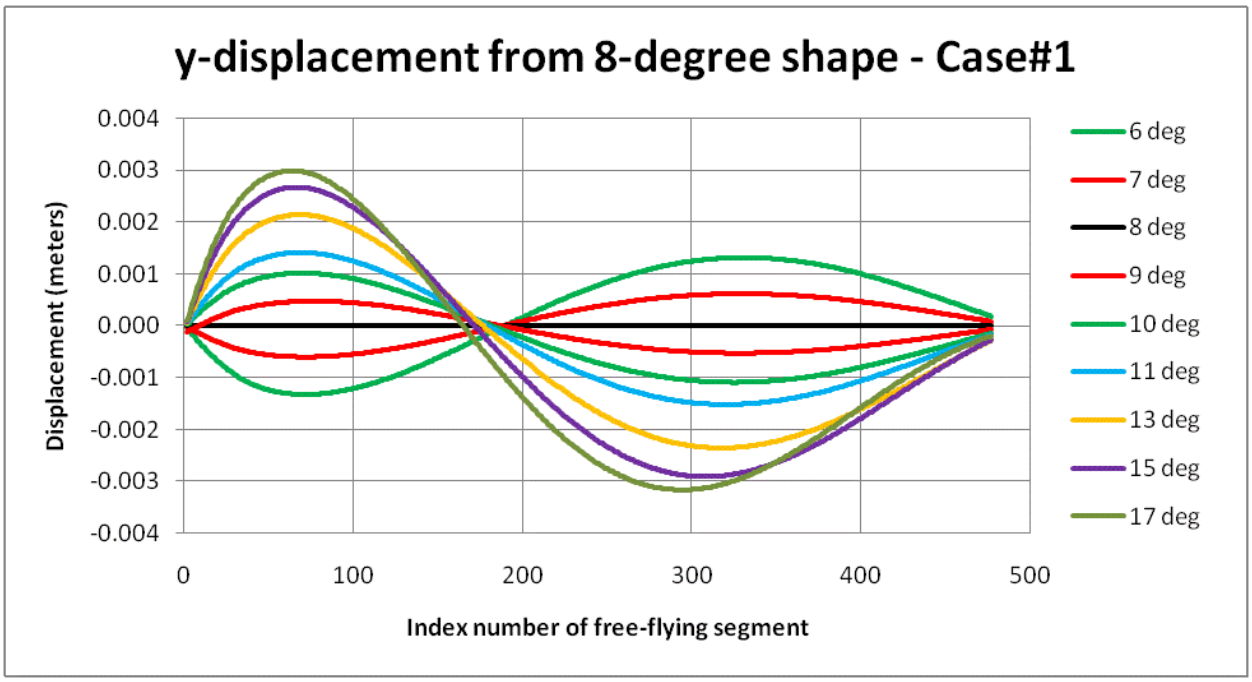

Note that the curves in the previous graph are not the shape of the membrane *per se*, but rather the difference in shape from that at the 8° angle of attack. As the angle of attack increases, the fore part of the membrane rises and the after part becomes flatter. This tends to move the point of maximum thickness / camber forward as the angle of attack increases.

The following graph shows the lift and drag, measured in Newtons of force per spanwise meter, for this section at various angles of attack, and the corresponding lift-to-drag ratios. The lift and drag include the contributions from the leading edge tube.

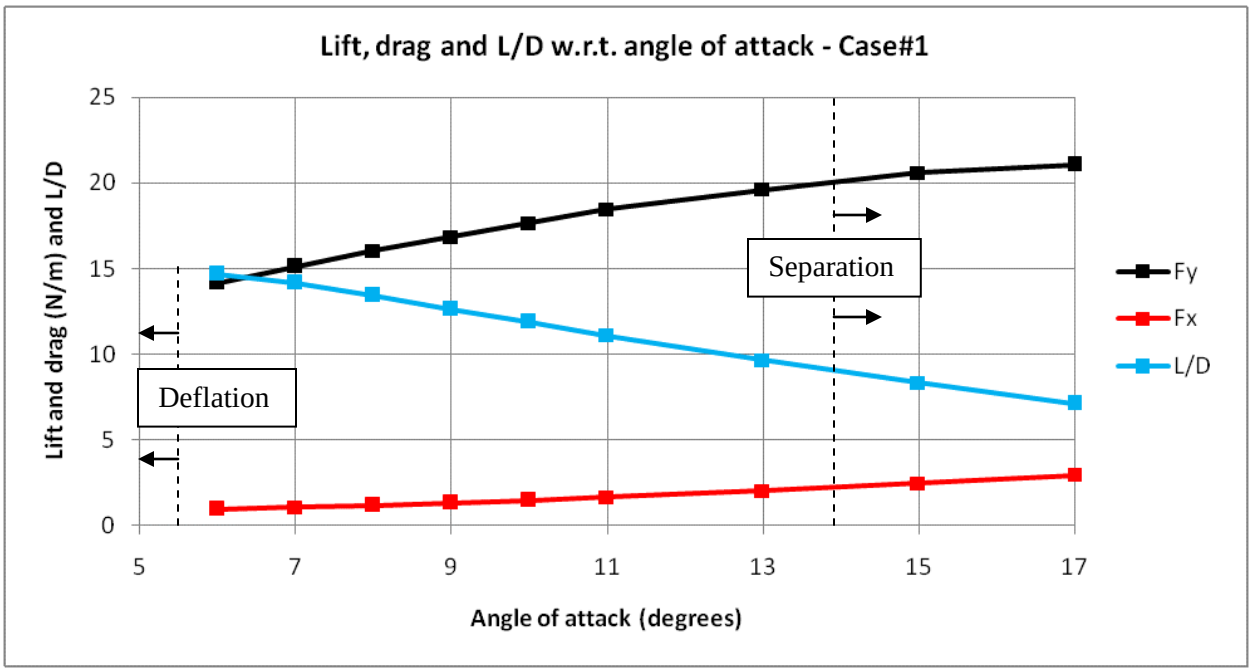

The lift curve does have the shape of a classical airfoil, which is to say, a sine curve. At low angles of attack, the lift curve is approximately linear. It looks as if it reaches the sinusoidal maximum at an angle of attack of 17°, or perhaps a little more. The drag increases with increasing angle of attack, with a slight non-linear tendency towards greater-than-linear increases in drag. Dividing the lift by the drag gives the lift-to-drag ratio, which deceases across the range of angles of attack studied. This occurs because the drag increases at a faster rate than the lift. (The lift-to-drag ratios are higher than I had expected. On the other hand, the section modeled has an infinite span. The wing-tip corrections for a finite span will reduce the overall L/D ratios.)

If I had to choose a design angle of attack from this data alone, I would probably pick 9°. My biggest concern as a kite-flier is loss of control, and 9° seems far enough from deflation without too much reduction in lift-to-drag ratio.

The next graph shows how the tension in the free-flying part of the membrane changes with the angle of attack. The graph shows the magnitude of the tension and the angle which the tension vector makes with the reference chord. The magnitude and angle are plotted both at the departure point, where the nylon membrane leaves the surface of the leading edge tube, and at the trailing edge strings. The magnitudes are scaled to the axis on the left-hand side of the graph; the angles are scaled to the axis on the right-hand side. The increase in magnitude as the angle of attack increases is entirely consistent with the increase in lift and drag forces, which pull harder and harder on the nylon sheet. The increase in the leading edge

angle is also consistent -- the aerodynamic forces tend to pull the membrane upwards and away from the leading edge tube.

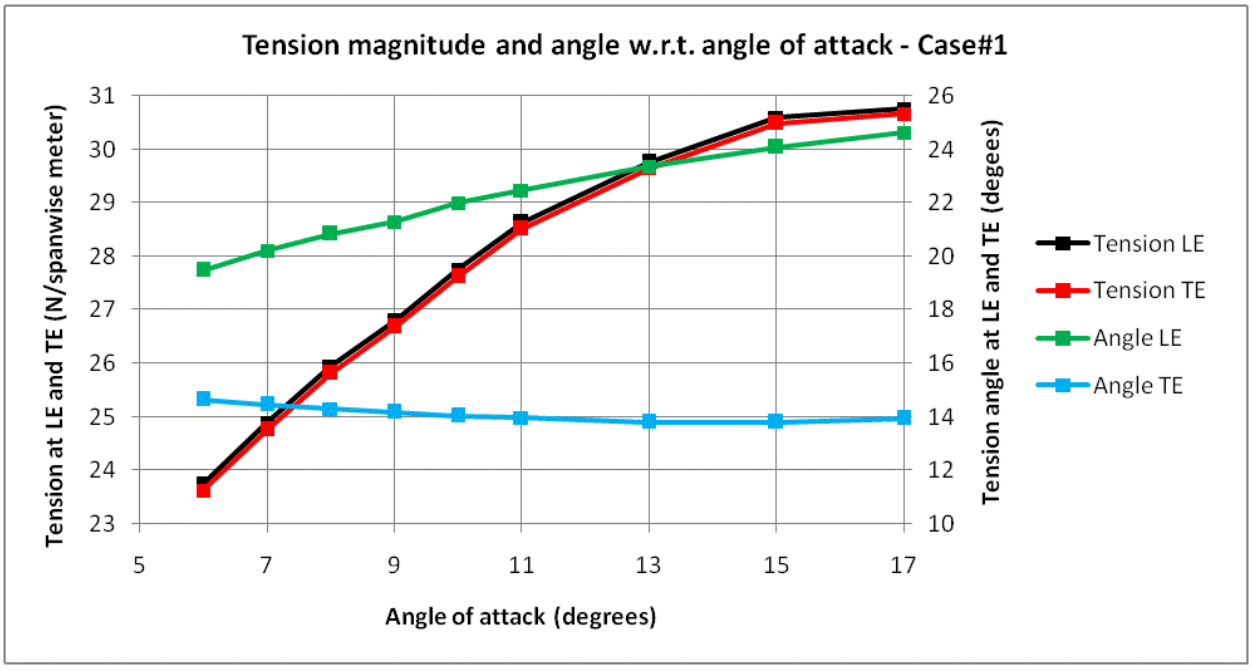

The next step in the analysis is to look at constructing the bridle to put the kite into static equilibrium. There is a quirk which needs disclosure first. The kite will be in static equilibrium if the sum of all the forces acting on it in the vertical direction are zero. Since there is no net force in the vertical direction, there will be no tendency for the kite to accelerate upwards or downwards to a different altitude. Static equilibrium also requires that there be no net force in the horizontal direction, which would otherwise cause the kite to accelerate upwind or downwind. Lastly, static equilibrium requires that there be no met moment, which would otherwise tend to accelerate the kite rotationally to a different angle of attack.

The net moment acting on the kite arises from three sources. There are the forces of gravity acting on the physical components of the kite. Since gravity always acts straight downwards, the forces due to gravity tend to rotate the kite clockwise. The tension forces which the nylon membrane exerts on the departure point and the trailing edge will tend to rotate the kite one way or the other, depending on their relative magnitudes and angles. The third source of moments are the aerodynamic forces acting on the leading edge tube itself. Since the leading edge tube is small compared with the membrane, the aerodynamic forces exerted directly on it are relatively small as well. (They are nevertheless included in the lift and drag figures plotted above.) The aerodynamic moment acting directly on the leading edge tube is also very small. The following graph shows for Case #1 the aerodynamic moment acting on the leading edge tube. The quirk at 8° is obvious.

It took me a while to identify the source of this quirk. Recall that the entire 98 centimeter length of the nylon membrane was discretized into 500 segments. That includes the two dozen or so segments which lie on the surface of the leading edge tube. One assumption made in the coding is that the departure point, at which the membrane breaks free from the surface of the tube, must coincide with one of the hinges which marks the point of contact between adjacent segments in the membrane. The calculations which take place at angles of attack of 7° and 9° are such that there were always 23 segments of nylon on the leading edge tube with the remaining 477 segments being free-flying. The calculations for 8° took a slightly different path. Between iterations #1 and #2 in the overall procedure, the shape calculation routine determined that the departure point should occur at the 25th hinge, at the downwind edge of the

24th segment. Subsequent iterations left it there. The distribution of forces in the subsequent iterations never became great enough to cause the departure point to return to the 24th hinge. This meant that the configuration for the 8° angle of attack was slightly different than all the others. The moment for this angle of attack is about one milli-Newton out of the trend set by the others. The effect is quite minor, and would likely disappear if the size of the segments was decreased. (The Case #2 runs did not show this anomaly.)

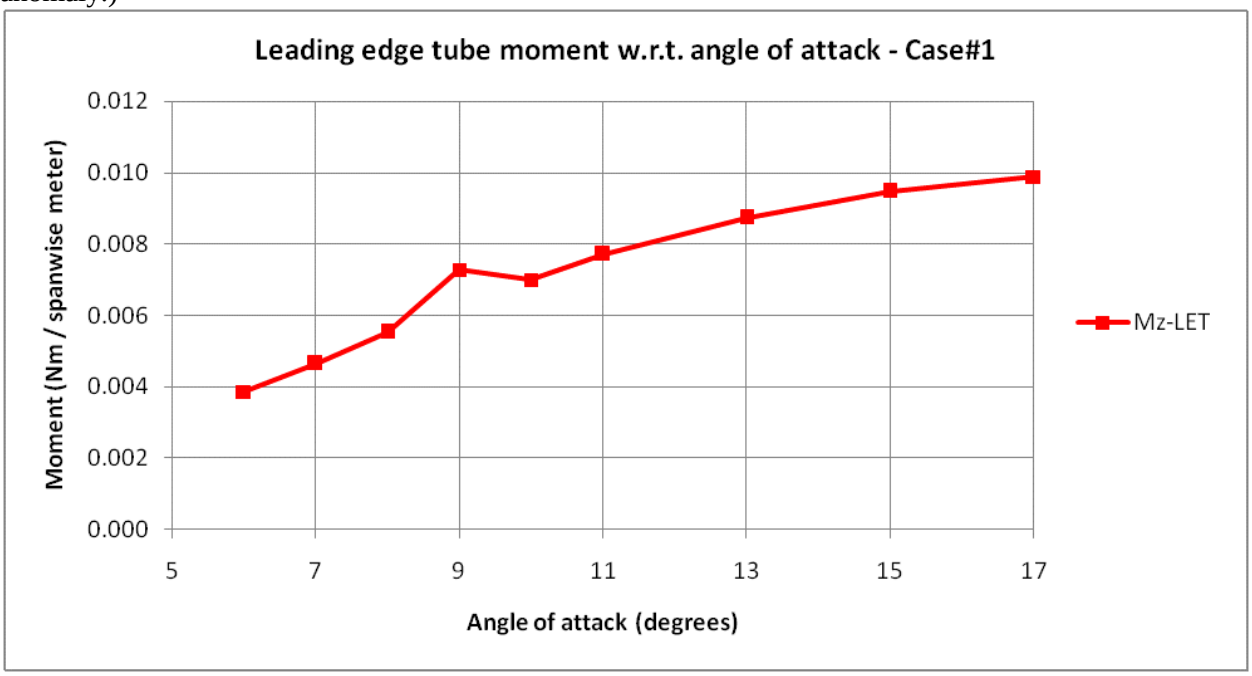

The equations and assumptions in Appendix "B" of the earlier paper were used to calculate the configuration of bridles which resulted in static equilibrium at these different angles of attack. I used as the two independent variables the length of the fore bridle line and the angle which the fore bridle line makes with respect to the underside of the reference chord. The length of the rear bridle line and the angle it makes with the underside of the reference chord are uniquely determined for any pair of independent variables. The following graph shows the equilibrium curves.

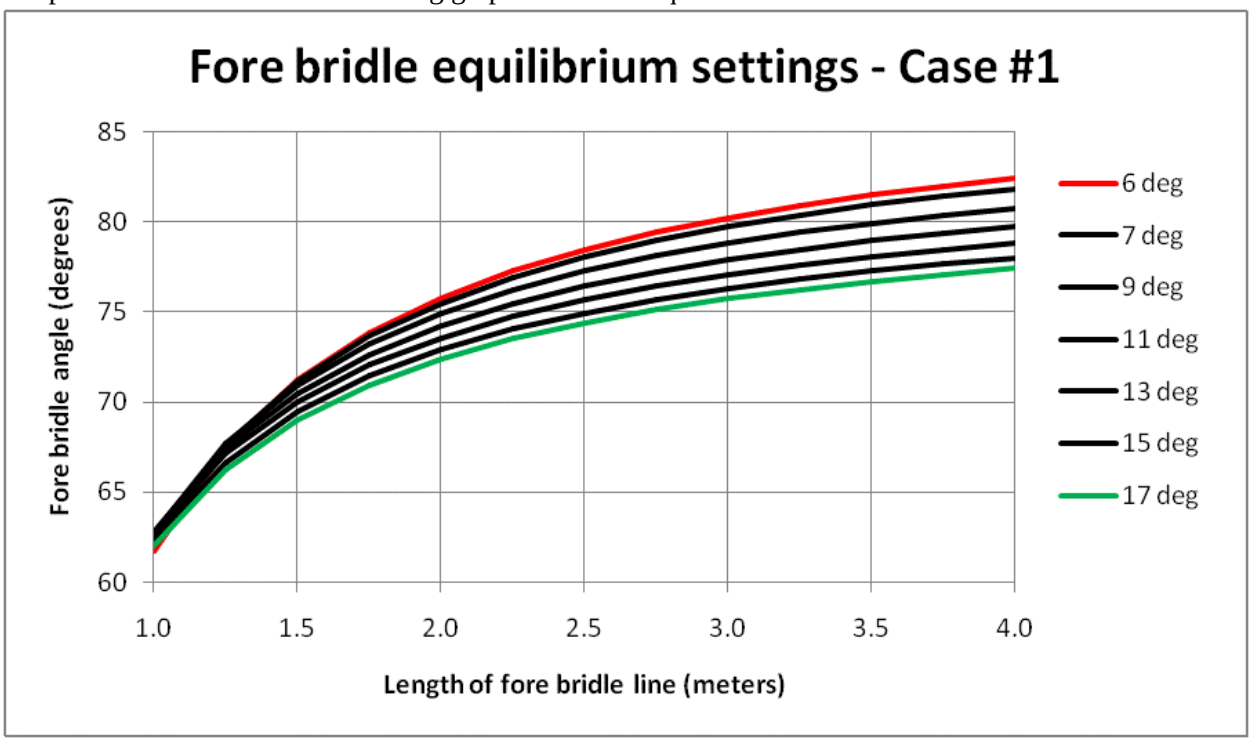

There is not a single setting for each individual angle of attack. Rather, there is a range of possibilities, each of which is consistent with static equilibrium. The following picture puts one of the curves in the preceding graph into its physical context. It shows the equilibrium possibilities for a single angle of attack, 9°.

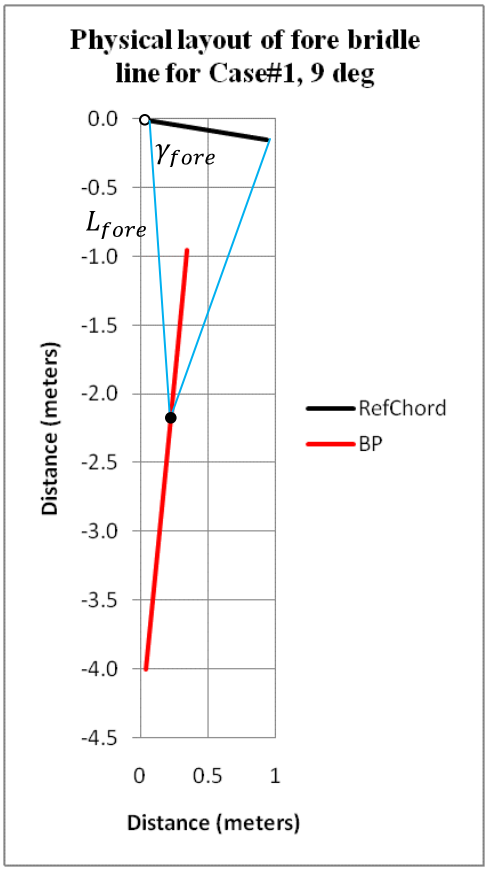

The black line is the reference chord, which is depressed from the horizontal by the 9° angle of attack. The reference chord is 94.54 cm long, being the 2.54 centimeter diameter of the leading edge tube plus the 92 cm length of the ribs. The small open dot at the leading edge is intended to represent the leading edge tube.

The two blue lines are rendered in blue. They meet at the bridle point BP, which is the small black dot. The particular bridle configuration shown has fore bridle length L_{fore} and fore bridle angle γ_{fore}. This combination of L_{fore} and γ_{fore} puts the kite into a static equilibrium. But, so does every other point along the red curve. The red curve is the loci of bridle points which represent static equilibrium.

I have taken some pains to scale both axes in this graph so that they represent the same physical length. What is shown therefore is a reasonably accurate side view of the kite-bridle system.

Results for Case #2, at 15,000 feet in a 20 mph wind

In Case #2, the same kite section was tested at an altitude of 15,000 feet, with a wind speed of 20 mph. Once again, the objective was to examine the section over a range of angles of attack. In this case, the range tested was from 6° to 17°. The OpenFoam simulation failed to converge at an angle of attack of 6°, which I interpreted as the onset of deflation. The following graph shows the trajectory of the residuals during the second OpenFoam simulation at 6°.

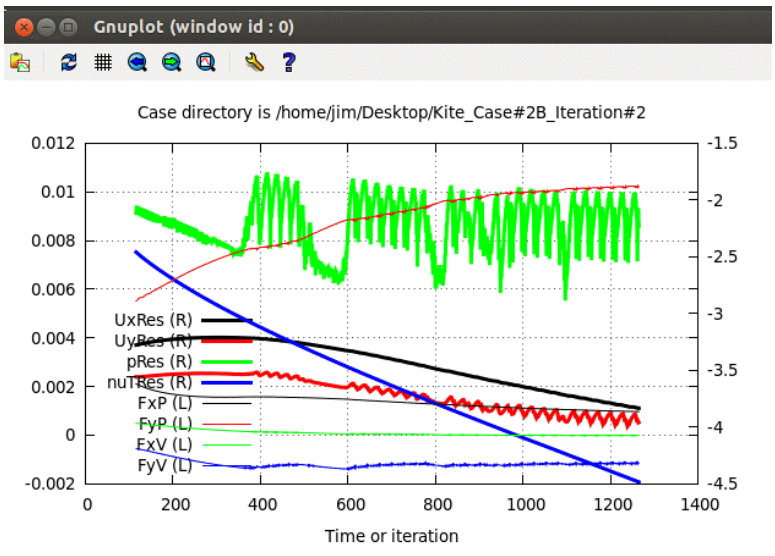

The incipient stall is illustrated in the following two pictures. They shows the streamtracers around the section at angles of attack of 15° and 17°, respectively. Once again, I would not willingly fly a kite which is this close to a stall.

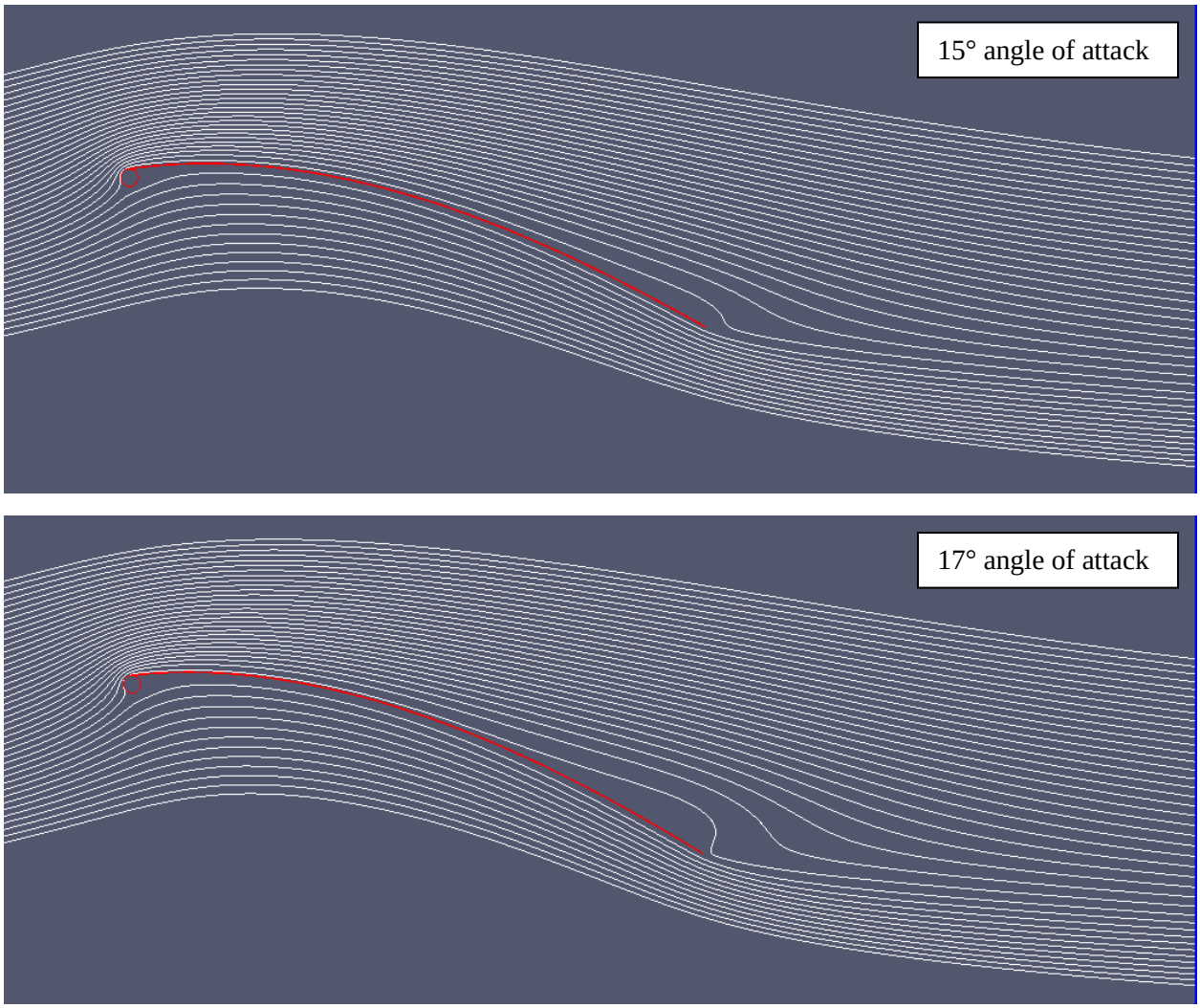

So, for Case #2, I restricted my attention to the range of angles of attack from 7° to 17°.

he following graph shows the lift and drag, measured in Newtons of force per spanwise meter, for this section at various angles of attack, and the corresponding lift-to-drag ratios. As before, the lift and drag forces include the contributions from the leading edge tube. Generally speaking, the characteristics of these curves is the same as those for Case #1. The magnitudes of the lift and drag forces are about one-half of what they were in Case #1. The increase in wind speed, from 10 mph in Case #1 to 20 mph in Case #2, offset some of the reductions resulting from lower density at high altitude.

I have added some information about the slopes of the lines. In due course below, I am going to examine the response of the kite to small changes from its static equilibrium. For that purpose, I am going to select an "operating condition" which I will select as the 9° angle of attack. At the 9° angle of attack, the lift and drag are 10.586 N/spanwise meter and 0.8912 N/m, respectively. In the neighbourhood of 9°, the lift and drag curves can be treated like straight lines, whose slopes are 0.532 N/m/degree and 0.0954 N/m/degree, respectively. I calculated these slopes by taking the difference between the lifts and drags at

angles of attack of 10° and 8°, and dividing by the two-degree difference in the angle of attack. The line segments I used to calculate these two slopes are shown as the heavy orange lines.

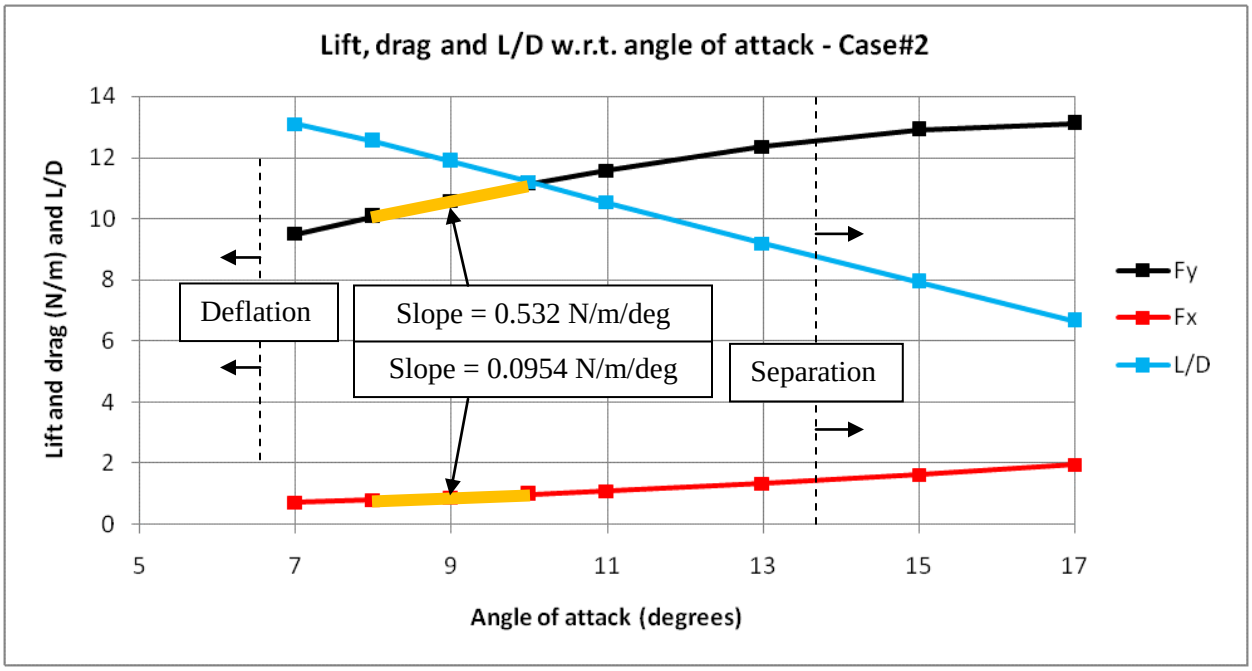

The next graph shows how the tension in the free-flying part of the membrane changes with the angle of attack. The graph shows the magnitude of the tension and the angle which the tension vector makes with the reference chord, at both the departure point and at the trailing edge. Generally speaking, these curves for Case #2 are qualitatively the same as the corresponding curves for Case #1.

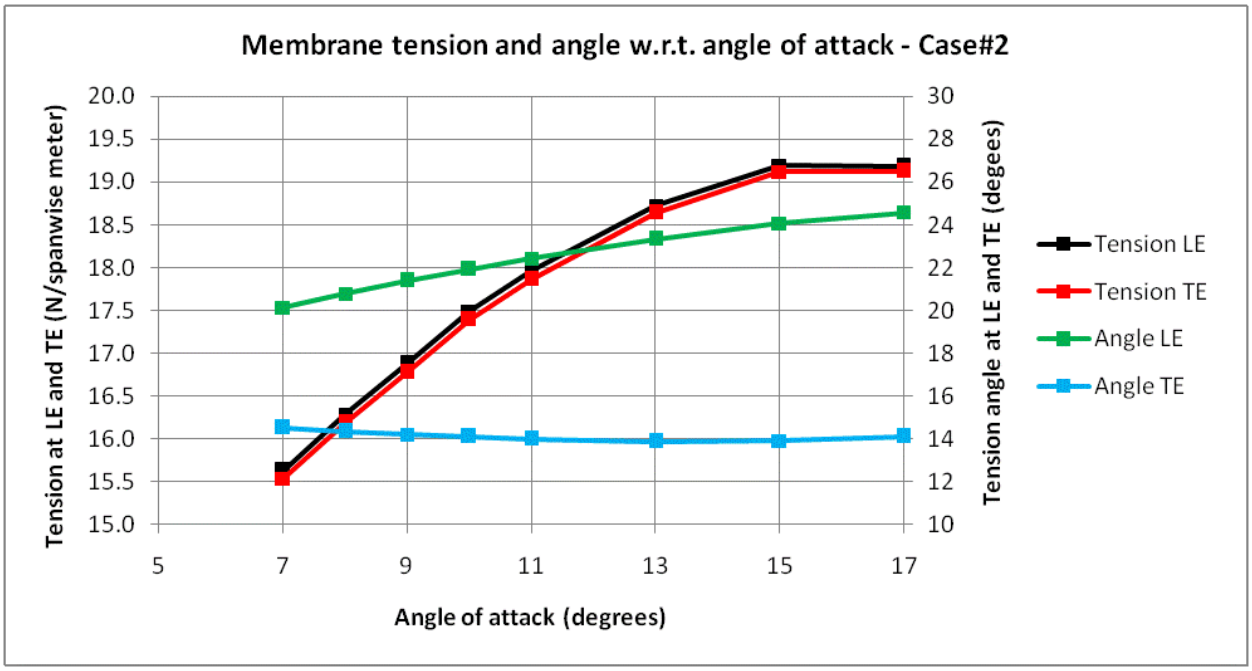

The following graph shows the settings for the fore bridle line which result in equilibrium for the kite in Case #2. These curves are extremely close to the corresponding curves for Case #1, as I will demonstrate shortly.

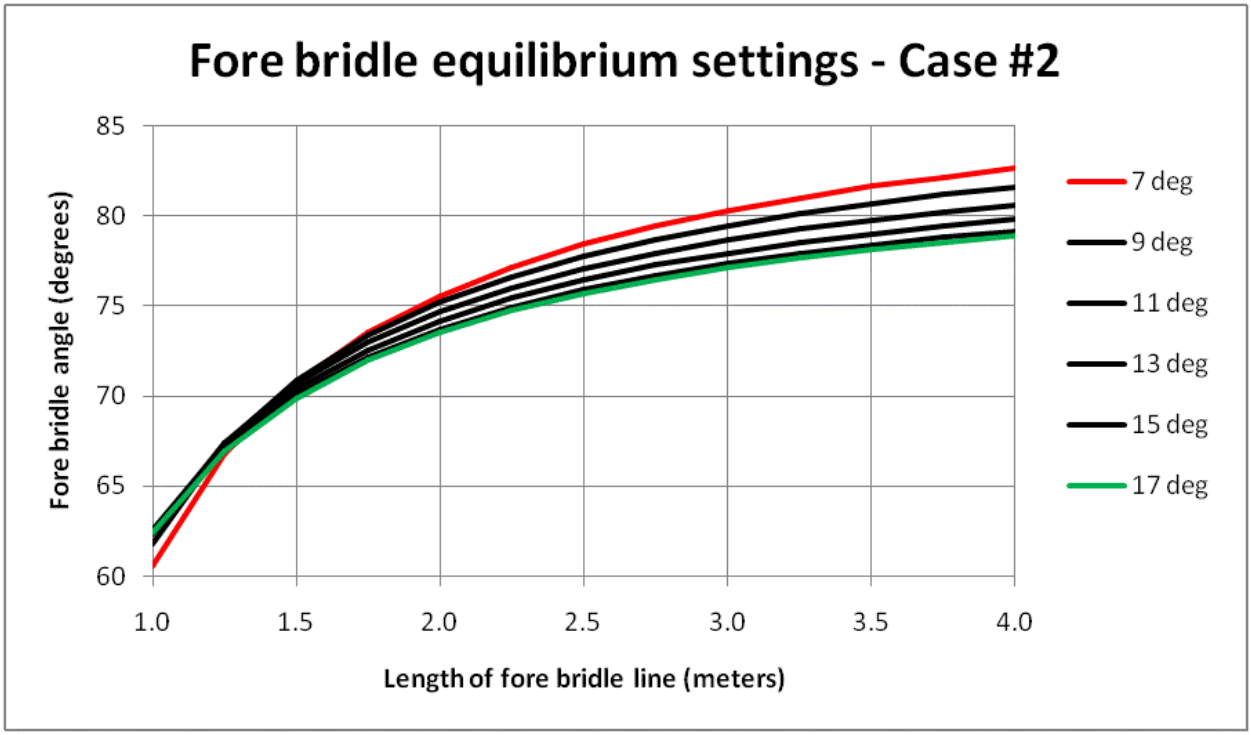

In the following graph, I compare certain of the equilibrium settings for the fore bridle line taken from the two Cases.

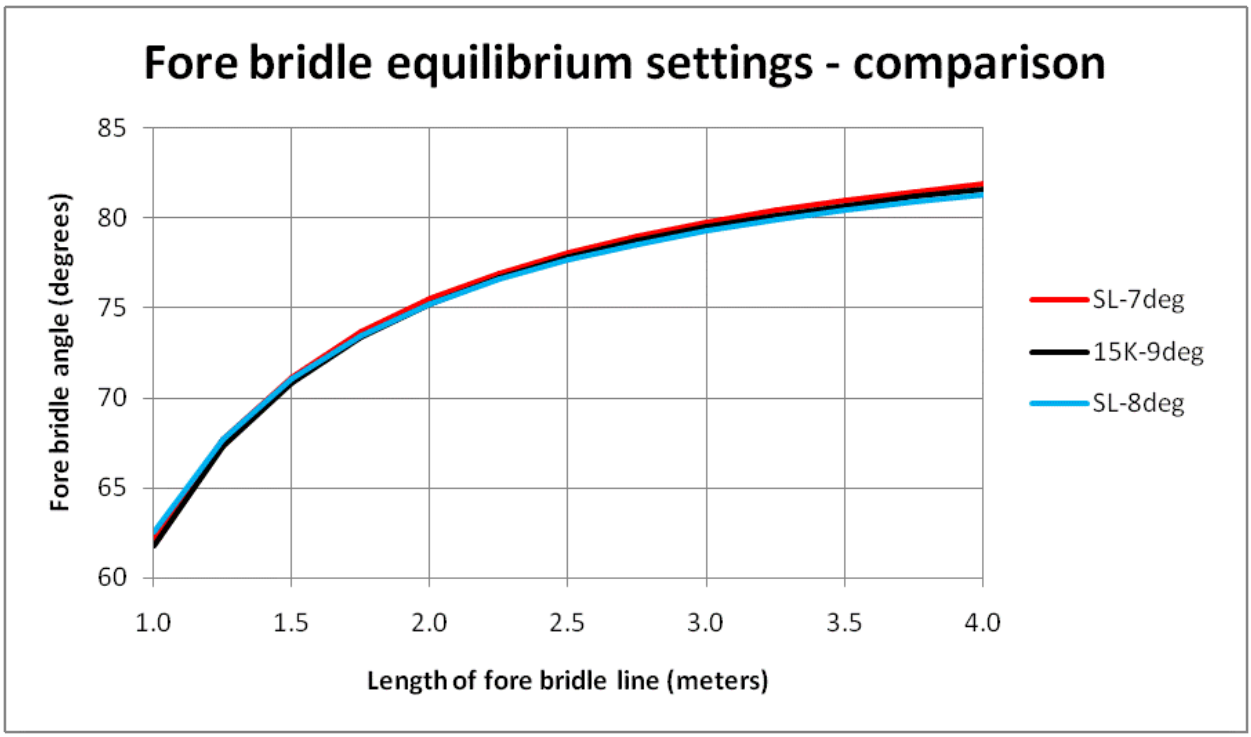

The red and blue curves are the bridle line settings at sea level (i.e., Case #1) for angles of attack of 7° and 8°, respectively. The black curve is the bridle line setting at 15,000 feet (i.e., Case #2) for an angle of attack of 9°. The two former curves bound the 15,000 foot curve, above and below, at least for fore bridle

lengths greater than about two meters. The physical implication is this: if one trims the kite on the ground for an angle of attack of about 7½°, it will fly at 9° once it reaches 15,000 feet.

The curves seem to coincide when the fore bridle line is about 1.5 meters. Generally speaking, the same coincidence at 1.5 meters occurs for all angles of attack in both flight conditions. This coincidence has a serious, and unfavourable, physical meaning. Let me state it this way. If the fore bridle line has a length of 1.5 meters (assuming that is the length which corresponds to the coincidence point), then the fore bridle angle can be set to bring the kite into static equilibrium at an angle of attack of 7°, for example. But that is also the setting which brings the kite into static equilibrium at 8°. And at 9°, and so on. What distinguishes between the various angles of attack. How does the kite choose one of the angles and not the others?

I think we have encountered the issue of stable equilibrium, not to be confused with static equilibrium. A static equilibrium exists when all the external forces and moments acting on the kite balance each other out. So long as this balance is exactly maintained, the kite will remain motionless. However, nothing in real life is perfectly constant. There will always be small (or large) changes in the flight conditions which will cause small (or large) changes in the forces acting on the kite. If the changes are small, one calls them "perturbations". If a perturbation jostles the kite slightly out of its static equilibrium condition, will it tend to return to the equilibrium condition, or not? If the kite exhibits a tendency to return to the static equilibrium condition, then the equilibrium is said to be stable. There are settings of the fore bridle line which are unstable. If the kite is perturbed from an unstable equilibrium, control will be lost.

The translational response of the kite to a perturbation in its angle of attack

Assume that the kite is flying in a static equilibrium at 15,000 feet at an angle of attack of 9°. Something happens, perhaps a gust of wind or a cold pocket of low density air, which drives the kite into a slightly different angle of attack, say 8½° or 9½°. The kite will no longer be in equilibrium. The net force acting in the vertical direction will not be zero, so the kite will tend to climb or sink in altitude. The net horizontal force on the kite will no longer be zero, so it will tend to move upwind or downwind. The net rotational moment on the kite will no longer be zero either, so the kite will tend to rotate to a new angle of attack as well. For these purposes, the "kite" I am referring to includes the bridle lines. Until will find otherwise, I will assume that the two bridle lines each remain in tension, so the bridle "triangle" remains rigid.

Figuring out how the net forces change is much easier than figuring out how the net moment changes, so I will consider only the forces, and not the moment, in this section. Changes in the forces result in translation, or linear motion, of the kite.

Let's first identify what changes and what doesn't change immediately after the kite is jostled out of its equilibrium attitude.

1. The gravitational forces, or weights, do not change.
2. The force exerted by the tether line on the bridle point does not change. To see this, observe that the kite can fly in an equilibrium condition only if the entire tether line is also in equilibrium. The tether is subjected to gravity and aerodynamic forces which affect the shape it adopts. It is held up at its upper end by the kite, whose bridle lines are attached to the tether at the bridle point. The forces which the kite exerts on the tether and tether exerts on the kite are equal and opposite. The kite's being jostled out of its equilibrium does not immediately affect the tether, which continues to pull down with the same force as before.

3. The forces in the fore and rear bridle lines will change. If we are treating the kite-bridle system as a rigid body, however, we do not need to inquire into this change. We can treat it as an internal stress inside the rigid body, whose overall dynamics are governed by externally-applied forces only.

4. The aerodynamic forces are the only ones which change.

The lift and drag forces plotted in the graphs above are complete, in the sense that they include all of the aerodynamic effects. We can therefore use the slopes of the lift and drag curves in the neighbourhood of the equilibrium angle of attack to calculate the net force which obtains at a perturbed angle of attack. Recall from above that the slopes of the lift and drag curves at a 9° angle of attack were given as 0.532 N/m/degree and 0.0954 N/m/degree, respectively. The following table sets out the net upwards force (lift) and net downwind force (drag) on the kite at slightly different angles of attack.

	8½° angle of attack	9° angle of attack	9½° angle of attack
Net upwards force (N/m)	$0.532 \times -½ = -0.266$	0	$0.5317 \times ½ = 0.266$
Net downwind force (N/m)	$0.0954 \times -½ = -0.0477$	0	$0.0954 \times ½ = 0.0477$

An increase in the angle of attack, from 9° to 9½°, causes an increase in both lift and drag, which will cause the kite to climb and to fly downwind. A decrease in the angle of attack by one-half degree causes an exactly opposite tendency, for the kite to descend and to fly upwind. I should emphasize that these are the tendencies which prevail at the instant after the perturbation occurs, but before the kite and tether line have begun to take responsive action.

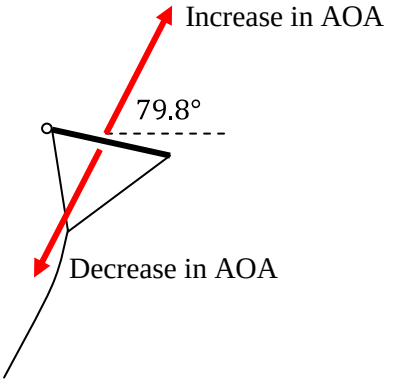

The ratio of the net upwards and net downwind forces are the same for increases and decreases in the angle of attack. In the neighbourhood of an equilibrium at 9°, they are $0.266/0.0477 = 5.58$. The arctangent of this ratio is the angle of the direction in which the kite will tend to accelerate. Here, it is $\tan^{-1} 5.58 = 79.8°$. The figure to the left illustrates with red arrows the direction in which the kite will start to accelerate following a perturbation to its 9° equilibrium.

The red arrows show the initial acceleration of the kite. Following through, and calculating the speed of the kite thereafter, is a very complicate problem of dynamics. It is not enough to simply integrate the acceleration to find the kite's velocity. The kite's own velocity changes the effective angle of attack, thus changing the membrane's shape and the aerodynamic forces. Not only that, but the kite can only move if it also moves the tether along with it. This involves moving the mass of the tether as well as counteracting the additional drag the tether line suffers as it, too, is dragged along.

Even though a complete analysis of the dynamics is beyond reach, we can do a quick calculation to put an upper bound on the size of the response. For this purpose, we will treat the kite as a point mass. In the earlier paper, we estimated its mass to be about 0.33 kilograms per spanwise meter. The net force after a one-half degree perturbation in the angle of attack is $\sqrt{0.266^2 + 0.0477^2} = 0.27$ Newtons per spanwise meter. Using Newton's Law, the acceleration is $a = F/m = 0.27/0.33 = 0.81\ m/s^2$. If the kite was a point mass then, after one second, it would have accelerated to a speed of 0.81 meters per second, primarily in the vertical direction. The true wind speed at equilibrium was 20 mph, or 8.94 meters per second. The figure below shows the relative winds which would prevail after one second.

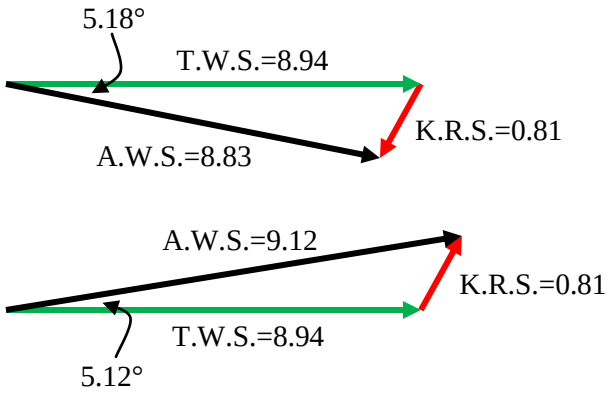

The green arrows represent the true wind speed, which is horizontal at 20 mph. The red arrows represent the kite's relative speed with respect to the air or, stated in reverse, the additional speed of the air resulting from the kite's speed. The top diagram applies to an increase in the angle of attack; the lower diagram applies to a decrease in the angle of attack. Lastly, the black arrow is the resultant of the two components of the air's speed, and is called the apparent wind speed.

Note that the apparent wind differs from the equilibrium wind in both speed and direction. In both cases, a perturbation by one-half degree gives rise to a 5° change in the angle of attack. In the case of a reduction in the angle of attack from 9° to 8½°, the kite travels down and into the wind, which increases the effective angle of attack by 5°.

Of course, these calculations greatly overestimate the speed the kite will attain after a perturbation to its angle of attack. It is important to note, though, that these changes to the apparent wind are in a direction which tends to restore the angle of attack to its pre-perturbation value.

I want to describe next the effect of a net non-zero moment on the kite's equilibrium. As I said above, the analysis of a net non-zero moment is more difficult than that of net non-zero forces. One could proceed in pretty much the same way as for the forces. That is, one could calculate slopes for the membrane's fore and aft tension forces and angles, and use those variations as the basis for calculating the changes in attitude. But, I will not go that route. I will not use the membrane tension as the starting point for the moment analysis. (Philosophically, the only reason the membrane tensions and angles are important in this study is because they are key ingredients to determining the shape. Once the shape is known for given angles of attack, and the corresponding lifts and drags calculated for them, we can circumvent use of the tensions.) Instead, I will base the moment analysis on two distances, to the center-of-gravity and to the center-of-pressure.

The center-of-gravity

In the earlier paper, I estimated the masses of the physical components (per meter of span) from which the kite could be built. For each component mass, I also estimated the point-of-action at which the gravitational force on it (i.e., its weight) could be assumed to act. The following table lists the component masses and weights, their points-of-action in the kite-fixed frame of reference and the moment which each weight exerts around the $(0, 0)$ origin. All of the point-of-action are assumed to lie on the reference chord, so the table only lists the x-direction displacement from the origin.

Component	Mass (g/m)	Weight (N)	POA x (m)	Moment (N)
Leading edge tube	165.67	1.62466	0.0127	0.02063
Ribs	22.97	0.22522	0.5254	0.11833
Nylon1	5.59	0.05478	0.0127	0.00070
Nylon2	64.41	0.63169	0.5254	0.33189
Forward hardware	49.21	0.48261	0.0254	0.01226
Aft hardware	24.61	0.24131	1.0254	0.24743
Total	332.45	3.26026	0.2243	0.73124

The kite has a mass of about one-third of a kilogram per meter of span, with a corresponding weight of 3.26 Newtons per meter of span. The final column in the table above is the moment which the component's weights exert around the leading edge when the reference chord is held horizontal. In that configuration, the forces (weights) act downwards, at right angles to the x-displacements measured along the reference chord. Since the forces and their lever arms are perpendicular to each other, the mechanical moments are simply the product of the two. The total moment is about three-quarters of a Newton-meter, per meter of span. If one divides the total moment by the total weight, the resulting distance is the effective lever arm for the total weight. This distance is highlighted in yellow in the table. One can think of the total weight as being concentrated this distance (22.43 centimeters) aft of the leading edge. This location is the center-of-gravity. Its location along the reference chord is not affected by the angle of attack. See the following figure.

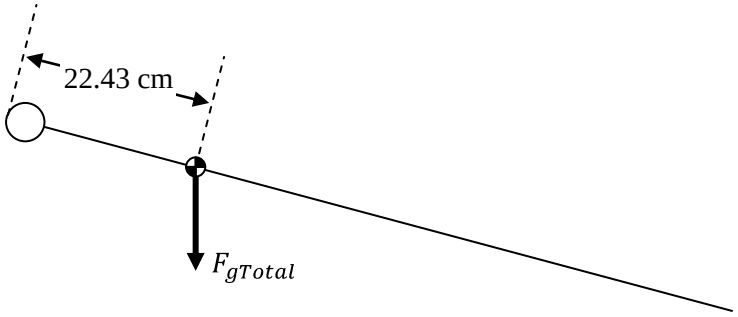

Conceptually, the center-of-gravity is the point at which we can imagine all of the gravitational forces to act, without the need for an accompanying explicit moment.

The center-of-pressure

The center-of-pressure has a similar purpose as the center-of-gravity. It is the point at which we can imagine all of the aerodynamic forces to act, without the need for an accompanying explicit moment. Unlike the gravitational forces, the aerodynamic forces (i.e., the lift and drag) do change as the angle of attack changes. Unlike the center-of-gravity, therefore, the center-of-pressure is not a fixed point, but moves as the angle of attack changes.

The first thing I want to do is carry out an example, showing how one calculates the center-of-pressure. I will use the case of a 9° angle of attack, with a wind speed of 20 mph at an altitude of 15,000 feet. In the final OpenFoam simulation for this sub-case, the total forces and moment acting on the kite were reported to be the following:

$$\begin{aligned} F_x &= 0.891 \text{ N/m} \\ F_y &= 10.586 \text{ N/m} \\ M_z &= 3.802 \text{ N} \end{aligned}$$

These figures include both the pressure-induced effects and the viscosity-induced effects. They include the effect of the leading edge tube as well as the nylon membrane. The co-ordinate frame of reference in which they are reported is the one used by OpenFoam, which has its x-axis parallel to the ground. The rotation axis around which the moment is calculated is the leading edge of the reference chord.

As is always the case, one can change the point-of-action at which a force is presumed to act, so long as an additional moment is added to compensate for the lever arm through which the force is moved. I am going to translate the forces a distance D_{cp} along the reference chord, from the leading edge, to a point at

which the compensating moment exactly offsets the moment reported by OpenFoam. The following figure shows the proposed translation.

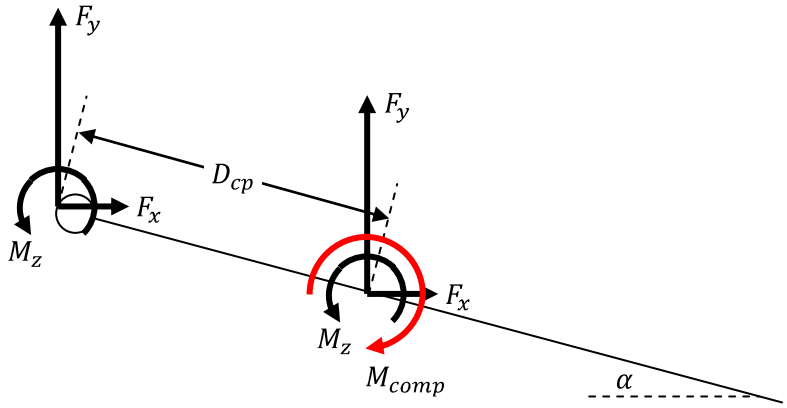

Note that the moment reported by OpenFoam is algebraically positive. It axis of rotation is therefore aligned with the positive z-axis, which points out of the page when the x- and y-axes have the directions shown. The moment tends to pitch the kite nose down.

To get a distance D_{cp} aft along the reference chord, the lift force F_y is translated to the right by a distance equal to $D_{cp}\cos\alpha$, where α is the angle of attack. If left uncompensated, force F_y would now exert an additional nose-down moment with magnitude $F_y D_{cp}\cos\alpha$. A compensating nose-up moment, in the direction of the red arrow, must be added to keep the toatls as they were stated before.

To get a distance D_{cp} aft along the reference chord, the drag force F_x is translated downwards by a distance equal to $D_{cp}\sin\alpha$. If left uncompensated, it too would exert an additional nose-down moment, with magnitude $F_x D_{cp}\sin\alpha$. A further compensating nose-up moment, also in the direction of the red arrow, must be added to preserve the totals.

The magic point we are looking for is the one at distance D_{cp} which results in the compenstaing moment being exactly equal and opposite to the aerodynamic moment. At this point, we will have the following equality:

$$\begin{aligned} & M_{comp} = M_z \\ \rightarrow \quad & F_y D_{cp}\cos\alpha + F_x D_{cp}\sin\alpha = M_z \\ \rightarrow \quad & D_{cp} = \frac{M_z}{F_y\cos\alpha + F_x\sin\alpha} \qquad (1) \end{aligned}$$

The numerical value of D_{cp} for the numerical example is:

$$D_{cp} = \frac{3.802}{10.586\cos 9° + 0.891\sin 9°} = 0.359 \text{ meters}$$

The point which is this distance aft along the reference chord is called the center-of-pressure.

The following figure shows the result when we repeat this calculation for other angles of attack. The red curve is the result for Case #2, that is, flight at 15,000 feet with a 20 mph wind speed. The black curve is the result for Case #1, a 10 mph wind speed at sea level.

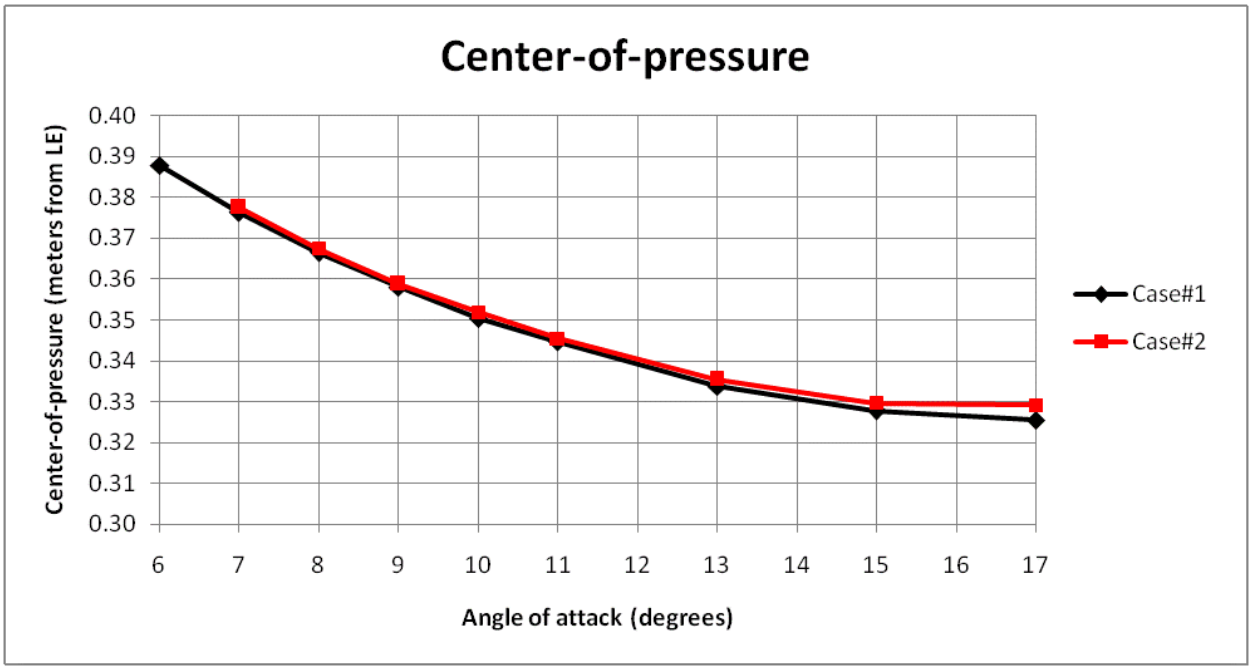

The vertical axis is worthy of note. It measures the distance to the center-of-pressure, aft along the reference chord from the leading edge. The entire range shown on the vertical axis is ten centimeters. The curves themselves cover a range of only six centimeters. This is quite a narrow range, given that the reference chord is approximately one meter long. In other words, the center-of-pressure remains almost constant over a wide range of flight conditions.

This phenomenon is also observed with conventional airfoils, for which the rule of thumb is that the center-of-pressure lies at the quarter-chord. For the thin highly-cambered kite section under study, one could propose a rule of thumb that the center-of-pressure is at 35% of chord. That is what we will assume for the following analysis of the net moment following a perturbation in the angle of attack.

The center-of-tether-tension

Three sets of external forces act on the kite-bridle body. By defining a center-of-gravity and a center-of-pressure, we have simplified our understanding of two of them, the gravitational and aerodynamic forces. The simplification consisted of placing the forces at points-of-action where their locations alone gave rise to the moments observed.

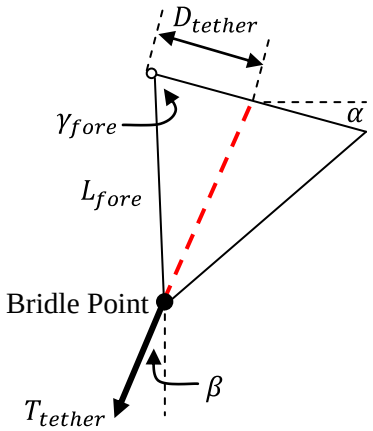

The third external force is the tension force in the tether line. It, too, gives rise to a mechanical moment around the kite's leading edge. And, like the other two sets of external forces, we can seek a point-of-action on the reference chord where we can place the tether's tension force without the need for an explicit moment. The figure at the left shows the geometry we will use.

We will translate the tension T_{tether} along its line-of-acton, shown as the red dashed line, upwards to the point at which it intersects the reference chord. Since this force is being translated along its line-of-acton, the translation does not change the moment meaured around the leading edge / origin.

D_{tether} is defined in the figure as the distance from the leading edge to the center-of-tether-tension. In order to express that distance in terms of the other quantities, we have to work through a succession of triangles.

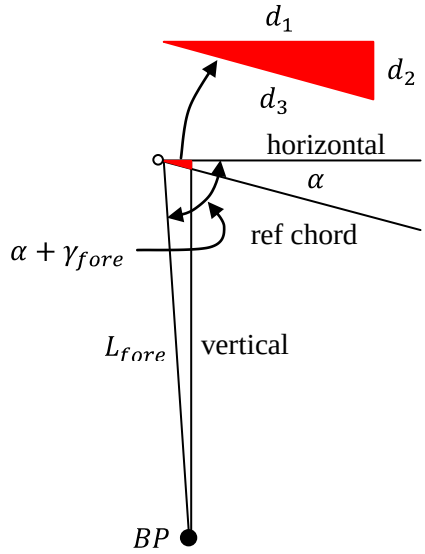

Let's begin with a small right triangle just aft of the leading edge tube, with one vertex at the point of intersection between the ribs and the leading edge tube. The subject triangle is rendered in red in the figure at the left. From trigonometry, we can see that:

$$d_1 = L_{fore}\cos(\alpha + \gamma_{fore}) \quad (2)$$

and

$$\begin{aligned} d_2 &= d_1 \tan\alpha \\ &= L_{fore}\cos(\alpha + \gamma_{fore})\tan\alpha \end{aligned} \quad (3)$$

Using the Pythagorean Theorem:

$$\begin{aligned} d_3 &= \sqrt{d_1^2 + d_2^2} \\ &= L_{fore}\cos(\alpha + \gamma_{fore})\sqrt{1 + \tan^2\alpha} \\ &= L_{fore}\frac{\cos(\alpha + \gamma_{fore})}{\cos\alpha} \end{aligned} \quad (4)$$

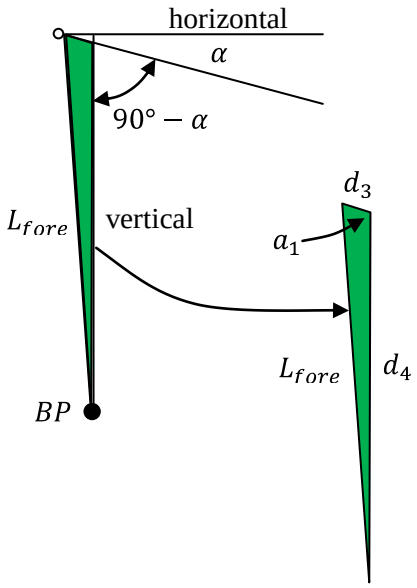

Now, let's look at the triangle shown here in green, which lies directly below the red triangle from above. The vertical distance d_4 can be calculated as follows:

$$\begin{aligned} d_4 &= L_{fore}\sin(\alpha + \gamma_{fore}) - d_2 \\ &= L_{fore}\begin{bmatrix} \sin(\alpha + \gamma_{fore}) + \cdots \\ \cdots - \cos(\alpha + \gamma_{fore})\tan\alpha \end{bmatrix} \\ &= L_{fore}\begin{bmatrix} \sin\alpha\cos\gamma_{fore} + \cdots \\ \cdots + \cos\alpha\sin\gamma_{fore} + \cdots \\ \cdots - \cos\alpha\cos\gamma_{fore}\tan\alpha + \cdots \\ \cdots + \sin\alpha\sin\gamma_{fore}\tan\alpha \end{bmatrix} \\ &= L_{fore}\begin{bmatrix} \cos\alpha\sin\gamma_{fore} + \cdots \\ \cdots + \sin\alpha\sin\gamma_{fore}\tan\alpha \end{bmatrix} \\ &= L_{fore}\frac{\sin\gamma_{fore}}{\cos\alpha} \end{aligned} \quad (5)$$

The obtuse angle a_1 can be found using the sine law for arbitrary triangles, in our case, thus:

$$\frac{\sin a_1}{L_{fore}} = \frac{\sin(90° - \alpha)}{d_4}$$

which can be re-arranged to give:

$$\sin a_1 = \frac{L_{fore}\cos\alpha}{L_{fore}\dfrac{\sin\gamma_{fore}}{\cos\alpha}}$$

$$\rightarrow \quad a_1 = \sin^{-1}\left(\frac{\cos^2\alpha}{\sin\gamma_{fore}}\right) \quad (6)$$

We can now more on to our third, and last, triangle. It is rendered in blue in the figure to the left.

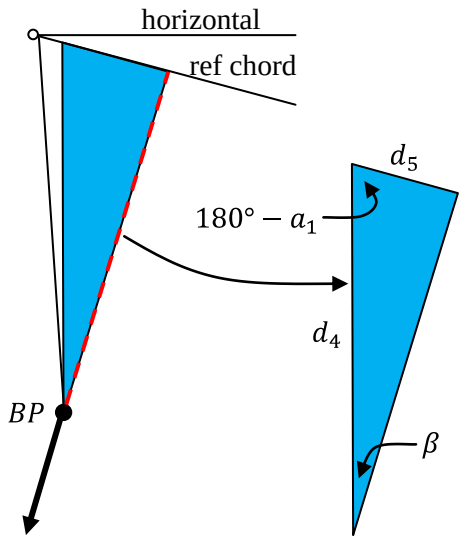

Despite its appearance in the figure, the blue triangle is not a right triangle. However, we do know two of its interior angles (β and $180° - a_1$) and one of its sides (d_4), which will be sufficient to calculate the others angle and sides. The quantity we are interested in is the distance d_5 along the reference chord. We will use the general sine law once again, in the following form:

$$\frac{\sin\beta}{d_5} = \frac{\sin[180° - (180° - a_1 + \beta)]}{d_4}$$

This can be solved for d_5 as follows:

$$d_5 = d_4\frac{\sin\beta}{\sin(a_1 - \beta)}$$

$$= L_{fore}\frac{\sin\gamma_{fore}\sin\beta}{\cos\alpha\sin(a_1 - \beta)} \quad (7)$$

We are now in a position to add up the component distances which give the distance along the reference chord to the center-of-tether tension. There are three components -- do not forget that the forward bridle line is attached to the kite at the point of intersection between the ribs and the leading edge tube. This point is aft of the leading edge by a distance equal to the diameter of the leading edge tube. The sum is:

$$D_{tether} = 2R_{LE} + d_3 + d_5$$

$$= 2R_{LE} + L_{fore}\frac{\cos(\alpha + \gamma_{fore})}{\cos\alpha} + L_{fore}\frac{\sin\gamma_{fore}\sin\beta}{\cos\alpha\sin(a_1 - \beta)} \quad (8)$$

Let's work our way through the quantities in our numerical example. Recall that the length of the fore bridle is four meters, the corresponding fore bridle angle $\gamma_{fore} = 81.617°$ and the tether line angle $\beta = 6.937°$ at an angle of attack of 9°. Then:

$$d_1 = 4\cos(9° + 81.617°) = -0.0431 \text{ m}$$

$$d_2 = 4\cos(9° + 81.617°)\tan 9° = -0.00682 \text{ m}$$

$$d_3 = 4\frac{\cos(9° + 81.617°)}{\cos 9°} = -0.0436 \text{ m}$$

The negative distance should not be alarming. They reflect the fact that, in this particular case, the fore bridle line actually extends upwind for the kite as well as downwards to the bridle point. The fore bridle line lies to the left of the vertical rather than to the right of the vertical, as assumed in the figures above.

Continuing on, we get:

$$\begin{aligned} d_4 &= 4\frac{\sin 81.617°}{\cos 9°} && = 4.0066 \text{ m} \\ a_1 &= \sin^{-1}\left[\frac{\cos^2 9°}{\sin 81.617°}\right] && = 80.423° \\ d_5 &= 4\frac{\sin 81.617° \sin 6.937°}{\cos 9° \sin(81.617° - 6.937°)} && = 0.5017 \text{ m} \end{aligned}$$

And, finally, the numerical value of the center-of-tether-tension is found to be:

$$D_{tether} = 2R_{LE} + d_3 + d_5 = 0.0254 - 0.0436 + 0.5017 = 0.4835 \text{ m}$$

D_{tether} is soley a matter of geometry. It is the spot on the reference chord where it intersects with the line-of-action of the tether tension. If the kite was rotated slightly nose-down, the point of intersection would move towards the trailing edge. The following graph shows how D_{tether} varies from the equilibrium distance of 48.35 centimeters as the angle of attack varies. Note carefully: the distances shown in the graph are the result of re-calculating the formulae in Equations (2) through (8) where the only variable changed is the angle of attack α. The distances for angles of attack other than 9°, which is the equilibrium point, are <u>not</u> the centers-of-tether-tension for those other angles since the kite is not assumed to be in equilibrium at those other angles. The purpose of this special-purpose graph will be explained in the next section.

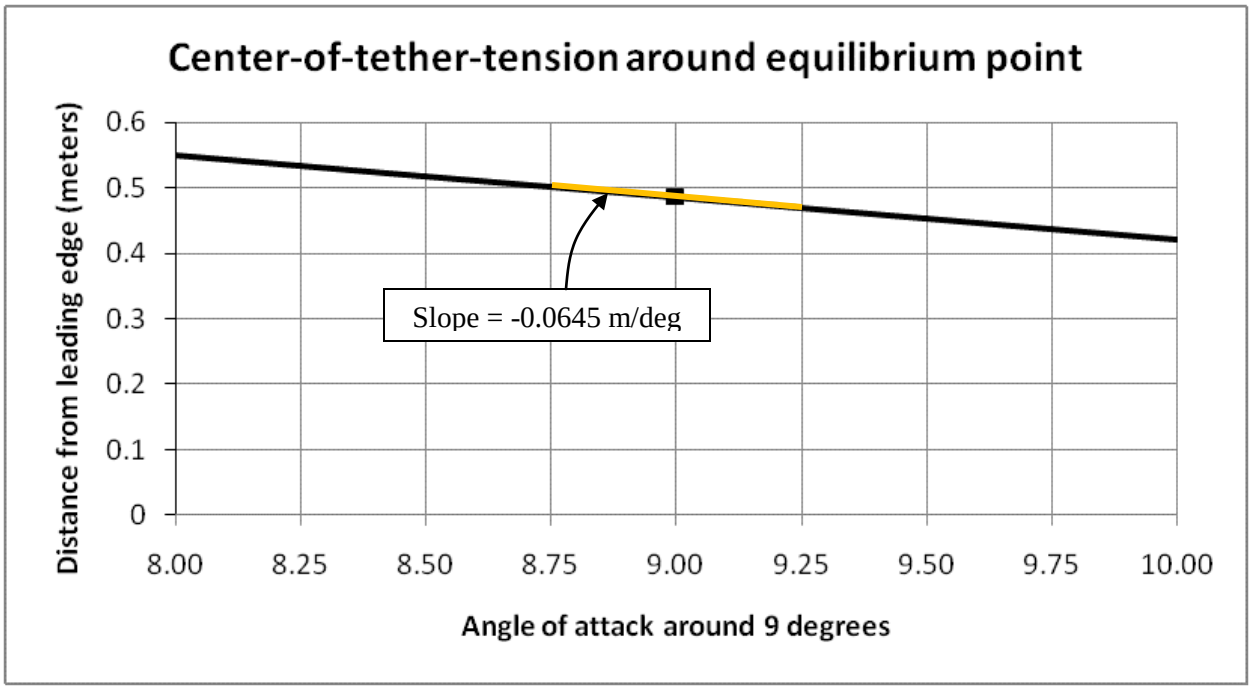

The curve may appear to be flat (and so there is not much fore-and-aft travel in the center-of-tether-tension), but that is because the entire horizontal range is only one degree less than to one degree greater than, the equilibrium angle of 9°. The negative slope of the curve confirms the expectation I described above, that a decrease in the angle of attack (nose-down) moves the projection point further aft. have also calculated the slope of the line in the neighbourhood of the equilibrium point.

The rotational response of the kite to a perturbation in its angle of attack

We are now in a position to consider the rotational response of the kite to a small perturbation in its angle of attack from an equilibrium state. The following diagram shows the free-body diagram for the kite in its equilibrium state. Numbers used in this section are from the same flight condition used as an example above, namely, 9° angle of attack, 15,000 foot altitude and a 20 mph wind speed. With the aid of the centers-of-gravity, pressure and tether tension, the free-body diagram does not need any explicit moments.

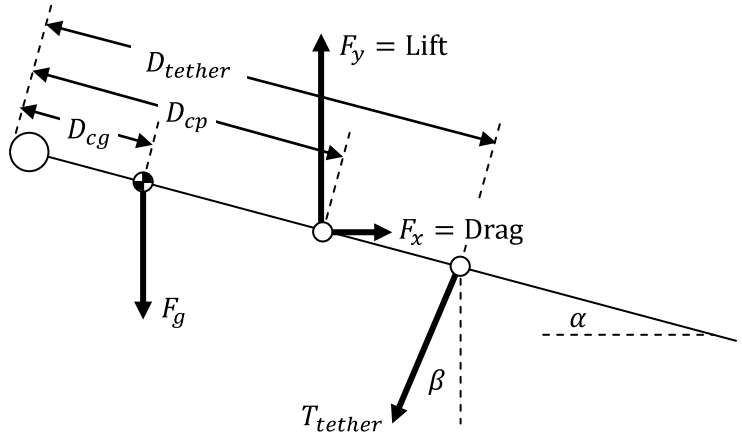

The kite is in equilibrium before the perturbation. The best way to say that mathematically is that the net moment, measured counter-clockwise around the center-of-gravity, must be zero. We can write down by inspection:

$$M_{ccw,cg}^{before} = \left\{ \begin{array}{c} F_y\left(D_{cp} - D_{cg}\right)\cos\alpha + \cdots \\ \cdots + F_x\left(D_{cp} - D_{cg}\right)\sin\alpha + \cdots \\ \cdots - T_{tether}\cos\beta\left(D_{tether} - D_{cg}\right)\cos\alpha + \cdots \\ \cdots - T_{tether}\cos\beta\left(D_{tether} - D_{cg}\right)\sin\alpha \end{array} \right\} = 0 \quad (9)$$

The following diagram shows the kite after a perturbation which increases the angle of attack by $\Delta\alpha$. I have tried to highlight in red the quantities which have changed.

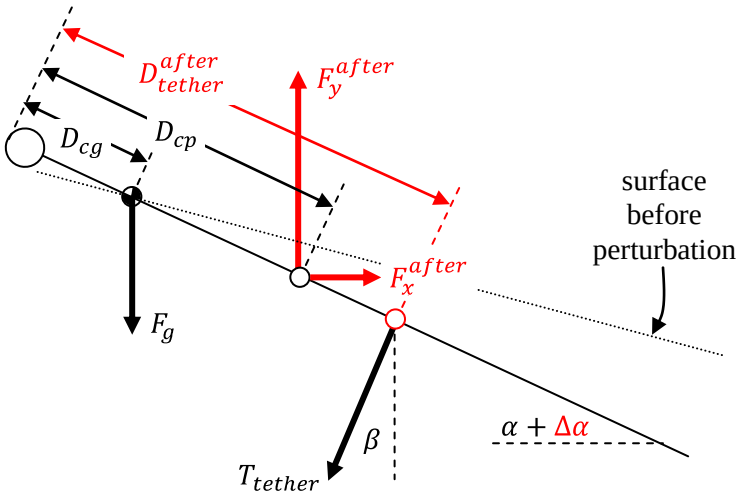

The new expression for the moment counter-clockwise around the center-of-gravity is as follows.

$$M_{ccw,cg}^{after} = \left\{ \begin{array}{c} F_y^{after}\left(D_{cp} - D_{cg}\right)\cos(\alpha + \Delta\alpha) + \cdots \\ \cdots + F_x^{after}\left(D_{cp} - D_{cg}\right)\sin(\alpha + \Delta\alpha) + \cdots \\ \cdots - T_{tether}\cos\beta\left(D_{tether}^{after} - D_{cg}\right)\cos(\alpha + \Delta\alpha) + \cdots \\ \cdots - T_{tether}\cos\beta\left(D_{tether}^{after} - D_{cg}\right)\sin(\alpha + \Delta\alpha) \end{array} \right\} \neq 0 \quad (10)$$

This moment will not be zero. In fact, it had better not be zero. If it is zero, then the kite will have no tendency to rotate after it has been knocked out of its equilibrium position. We do not want that. We want there to be a tendency to rotate, back towards the equilibrium angle of attack.

It is not necessary that we calculate the absolute magnitudes of the moments before and after. Knowing the change in the moment has more value. Let's define the change in the moment $\Delta M_{ccw,cg}$ as the moment after the perturbation less the moment before. Then:

$$\begin{aligned} \Delta M_{ccw,cg} &= M_{ccw,cg}^{after} - M_{ccw,cg}^{before} \\ &= \left\{ \begin{array}{c} F_y^{after}\left(D_{cp} - D_{cg}\right)\cos(\alpha + \Delta\alpha) + \cdots \\ \cdots - F_y\left(D_{cp} - D_{cg}\right)\cos\alpha + \cdots \\ \cdots + F_x^{after}\left(D_{cp} - D_{cg}\right)\sin(\alpha + \Delta\alpha) + \cdots \\ \cdots - F_x\left(D_{cp} - D_{cg}\right)\sin\alpha + \cdots \\ \cdots - T_{tether}\cos\beta\left(D_{tether}^{after} - D_{cg}\right)\cos(\alpha + \Delta\alpha) + \cdots \\ \cdots + T_{tether}\cos\beta\left(D_{tether} - D_{cg}\right)\cos\alpha + \cdots \\ \cdots - T_{tether}\cos\beta\left(D_{tether}^{after} - D_{cg}\right)\sin(\alpha + \Delta\alpha) + \cdots \\ \cdots + T_{tether}\cos\beta\left(D_{tether} - D_{cg}\right)\sin\alpha \end{array} \right\} \end{aligned} \quad (11)$$

I am going to process , and reduce, this expression by focusing on the first-order differences. As an alternative, one could use a lot of algebra to expand sub-expressions and collect terms. But that would disguise the key dependencies. I will use the following substitutions and first-order approximations:

$$F_y^{after} = F_y + \Delta F_y \quad (12A)$$
$$F_x^{after} = F_x + \Delta F_x \quad (12B)$$
$$D_{tether}^{after} = D_{tether} + \Delta D_{tether} \quad (12C)$$
$$\cos(\alpha + \Delta\alpha) \cong \cos\alpha - \Delta\alpha\sin\alpha \quad (12D)$$
$$\sin(\alpha + \Delta\alpha) \cong \sin\alpha + \Delta\alpha\cos\alpha \quad (12E)$$

The first three expressions are not so much approximations as they are definitions of certain differences. However, we will use these differences below as the "rise" component of the slopes which we would otherwise define using the Calculus. The last two expressions are the result of two steps. In the first step, $\cos(\alpha + \Delta\alpha)$ and $\sin(\alpha + \Delta\alpha)$ are expanded using the "sum of arguments" expansions. In the second step, $\Delta\alpha$ is assumed to be a small enough angle to allow us to use to use the "small angle approximations" that $\sin\Delta\alpha \cong \Delta\alpha$ and $\cos\Delta\alpha \cong 1$.

Substituting these expressions into Equation (11) and starting to simplify yields:

$$\Delta M_{ccw,cg} \cong \left\{ \begin{array}{c} \left(F_y + \Delta F_y\right)\left(D_{cp} - D_{cg}\right)(\cos\alpha - \Delta\alpha \sin\alpha) + \cdots \\ \cdots - F_y\left(D_{cp} - D_{cg}\right)\cos\alpha + \cdots \\ \cdots + \left(F_x + \Delta F_x\right)\left(D_{cp} - D_{cg}\right)(\sin\alpha + \Delta\alpha \cos\alpha) + \cdots \\ \cdots - F_x\left(D_{cp} - D_{cg}\right)\sin\alpha + \cdots \\ \cdots - T_{tether}\cos\beta\left(D_{tether} + \Delta D_{tether} - D_{cg}\right)(\cos\alpha - \Delta\alpha \sin\alpha) + \cdots \\ \cdots + T_{tether}\cos\beta\left(D_{tether} - D_{cg}\right)\cos\alpha + \cdots \\ \cdots - T_{tether}\cos\beta\left(D_{tether} + \Delta D_{tether} - D_{cg}\right)(\sin\alpha + \Delta\alpha \cos\alpha) + \cdots \\ \cdots + T_{tether}\cos\beta\left(D_{tether} - D_{cg}\right)\sin\alpha \end{array} \right\}$$

$$= \left\{ \begin{array}{c} -F_y\left(D_{cp} - D_{cg}\right)\Delta\alpha \sin\alpha + \cdots \\ \cdots + \Delta F_y\left(D_{cp} - D_{cg}\right)(\cos\alpha - \Delta\alpha \sin\alpha) + \cdots \\ \cdots + F_x\left(D_{cp} - D_{cg}\right)\Delta\alpha \cos\alpha + \cdots \\ \cdots + \Delta F_x\left(D_{cp} - D_{cg}\right)(\sin\alpha + \Delta\alpha \cos\alpha) + \cdots \\ \cdots + T_{tether}\cos\beta\left(D_{tether} - D_{cg}\right)\Delta\alpha \sin\alpha + \cdots \\ \cdots - T_{tether}\cos\beta\left(\Delta D_{tether}\right)(\cos\alpha - \Delta\alpha \sin\alpha) + \cdots \\ \cdots - T_{tether}\cos\beta\left(D_{tether} - D_{cg}\right)\Delta\alpha \cos\alpha + \cdots \\ \cdots - T_{tether}\cos\beta\left(\Delta D_{tether}\right)(\sin\alpha + \Delta\alpha \cos\alpha) \end{array} \right\} \qquad (13)$$

Observe that every term on the right-hand side is proportional to at least one "difference" like ΔF_y or $\Delta\alpha$. This is important. It means that the difference in the moment, being its change as a result of the perturbation, is quite a bit less than the moment itself. One would say that the change in the moment is itself a difference. Note that some terms are the product of two differences, such as $\Delta D_{tether}\Delta\alpha$. These are so-called second differences. Being the product of two (relatively small) differences, they are even an order smaller than the first-order differences.

In the next step, I will divide both sides of Equation (13) by the small change in the angle of attack. This assumes, of course, that the small change is not exactly equal to zero.

$$\frac{\Delta M_{ccw,cg}}{\Delta\alpha} \cong \left\{ \begin{array}{c} -F_y\left(D_{cp} - D_{cg}\right)\sin\alpha + \cdots \\ \cdots + \dfrac{\Delta F_y}{\Delta\alpha}\left(D_{cp} - D_{cg}\right)(\cos\alpha - \Delta\alpha \sin\alpha) + \cdots \\ \cdots + F_x\left(D_{cp} - D_{cg}\right)\cos\alpha + \cdots \\ \cdots + \dfrac{\Delta F_x}{\Delta\alpha}\left(D_{cp} - D_{cg}\right)(\sin\alpha + \Delta\alpha \cos\alpha) + \cdots \\ \cdots + T_{tether}\cos\beta\left(D_{tether} - D_{cg}\right)\sin\alpha + \cdots \\ \cdots - \dfrac{\Delta D_{tether}}{\Delta\alpha}T_{tether}\cos\beta\,(\cos\alpha - \Delta\alpha \sin\alpha) + \cdots \\ \cdots - T_{tether}\cos\beta\left(D_{tether} - D_{cg}\right)\cos\alpha + \cdots \\ \cdots - \dfrac{\Delta D_{tether}}{\Delta\alpha}T_{tether}\cos\beta\,(\sin\alpha + \Delta\alpha \cos\alpha) \end{array} \right\} \qquad (14)$$

There are four terms on the right-hand side which do not involve any differences. There is a close correspondence between these four terms and the four terms in Equation (9), which add up to the pre-perturbation moment $M_{ccw,cg}^{before}$. The differences are interesting: changes in the trigonometric functions

and some changes in sign. These clues might lead one to hypothesize that the four terms in Equation (14) are the derivative of the moment $M_{ccw,cg}^{before}$. And that is in fact the case. The four terms are the partial derivative of $M_{ccw,cg}^{before}$ with respect to the angle of attack. That this is so is borne out in the following expansion.

$$\begin{aligned}\frac{\partial M_{ccw,cg}^{before}}{\partial \alpha} &= \frac{\partial}{\partial \alpha}\begin{Bmatrix} F_y(D_{cp}-D_{cg})\cos\alpha+\cdots \\ \cdots+F_x(D_{cp}-D_{cg})\sin\alpha+\cdots \\ \cdots-T_{tether}\cos\beta\,(D_{tether}-D_{cg})\cos\alpha+\cdots \\ \cdots-T_{tether}\cos\beta\,(D_{tether}-D_{cg})\sin\alpha \end{Bmatrix} \\ &= \begin{Bmatrix} F_y(D_{cp}-D_{cg})\dfrac{\partial\cos\alpha}{\partial\alpha}+\cdots \\ \cdots+F_x(D_{cp}-D_{cg})\dfrac{\partial\sin\alpha}{\partial\alpha}+\cdots \\ \cdots-T_{tether}\cos\beta\,(D_{tether}-D_{cg})\dfrac{\partial\cos\alpha}{\partial\alpha}+\cdots \\ \cdots-T_{tether}\cos\beta\,(D_{tether}-D_{cg})\dfrac{\partial\sin\alpha}{\partial\alpha} \end{Bmatrix} \\ &= \begin{Bmatrix} -F_y(D_{cp}-D_{cg})\sin\alpha+\cdots \\ \cdots+F_x(D_{cp}-D_{cg})\cos\alpha+\cdots \\ \cdots+T_{tether}\cos\beta\,(D_{tether}-D_{cg})\sin\alpha+\cdots \\ \cdots-T_{tether}\cos\beta\,(D_{tether}-D_{cg})\cos\alpha \end{Bmatrix}\end{aligned} \qquad (15)$$

I must say that I did not expect this. In any event, it does allow us to re-write Equation (14) as follows:

$$\frac{\Delta M_{ccw,cg}}{\Delta\alpha} \cong \begin{Bmatrix} \dfrac{\partial M_{ccw,cg}^{before}}{\partial\alpha}+\cdots \\ \cdots+\left[\dfrac{\Delta F_y}{\Delta\alpha}(D_{cp}-D_{cg})-\dfrac{\Delta D_{tether}}{\Delta\alpha}T_{tether}\cos\beta\right](\cos\alpha-\Delta\alpha\sin\alpha)+\cdots \\ \cdots+\left[\dfrac{\Delta F_x}{\Delta\alpha}(D_{cp}-D_{cg})-\dfrac{\Delta D_{tether}}{\Delta\alpha}T_{tether}\cos\beta\right](\sin\alpha+\Delta\alpha\cos\alpha) \end{Bmatrix} \qquad (16)$$

Consider the three slopes which are highlighted in red on the right-hand side. $\Delta F_y/\Delta\alpha$, for example, is the change in the lift force which resulkts from a change in the angle of attack from the equilibrium point. We know this. It is the slope of one of the orange lines I overlaid on one of the graphs above. The other two slopes were also marked with orange lines in the graphs above. I have summarized their values, using the current notation, in the table which comes after the following graph.

The only term on the right-hand side which we do not yet know is the partial derivative. None of the graphs above show the moment acting on the whole kite. Take care – some of the graphs above do show a moment, but it is only the moment acting on the leading edge tube. The moments due to forces acting on the flexible part of the surface were taken into account when calculating the leading and trailing edge tensions exerted by the membrane. Our purpose is a little different now, and we need a graph showing the total aerodynamic moment acting on the surface as a function of the angle of attack. Such a graph is shown next.

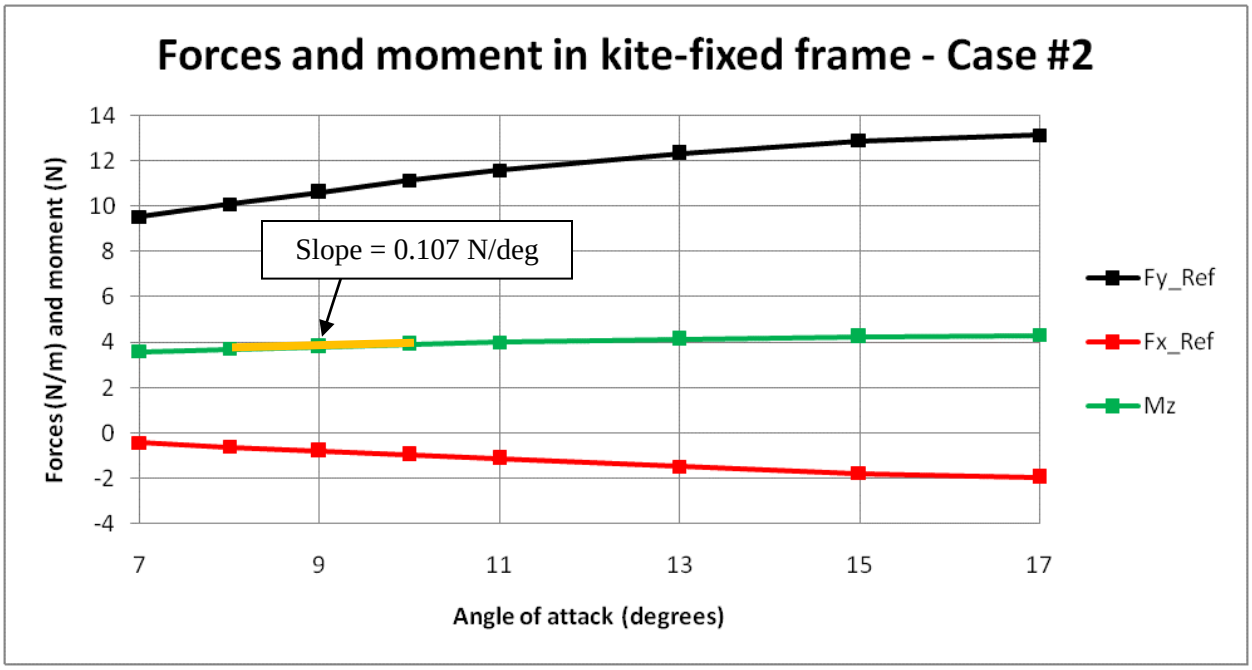

The graph shows the total aerodynamic force acting on the kite, as well as the total aerodynamic moment, at an altitude of 15,000 feet and a wind speed of 20 mph. The components of the total force should not be called the "lift" and "drag". In the graph, the two components are perpendicular to and parallel to the reference chord. The words "lift" and "drag" are reserved for the two components of the force when they are expressed perpendicular to and parallel to, respectively, the wind direction far upstream. The moment does not need a similar distinction – its value is the same in both frames of reference.

I should point out why the orange line segment is the partial derivative. By definition, a partial derivative with respect to one variable like α, is the change in the function which is caused by a change in this one variable only. All other variables are assumed to be held constant while this one variable changes. And that is what is shown in the graph. Only the angle of attack changes. Everything else – wind speed, altitude, component weights, tether tension, and so on – is constant or, at least, is not assumed to change.

The following table summarizes the four derivatives and equivalents in the right-hand side of Equation (16).

$$\frac{\partial M_{ccw,cg}^{before}}{\partial \alpha} = 0.107 \text{ N/deg}$$

$$\frac{\Delta F_y}{\Delta \alpha} = 0.532 \text{ N/m/deg}$$

$$\frac{\Delta F_x}{\Delta \alpha} = 0.0954 \text{ N/m/deg}$$

$$\frac{\Delta D_{tether}}{\Delta \alpha} = -0.0645 \text{ m/deg}$$

It is not necessary to crunch numbers before drawing a very important conclusion from Equation (16). Take a look at the algebraic signs.

$$\frac{\partial M_{ccw,cg}^{before}}{\partial \alpha} > 0$$
$$\frac{\Delta F_y}{\Delta \alpha} > 0$$
$$\frac{\Delta F_x}{\Delta \alpha} > 0$$
$$\frac{\Delta D_{tether}}{\Delta \alpha} < 0$$

It is very easy to explore the conditions under which the right-hand side of Equation (16) will be algebraically positive. The quantities which are definitely positive are circled. Let me work through the only possible risks to the right-hand side becoming negative.

$$\frac{\Delta M_{ccw,cg}}{\Delta \alpha} \cong \left\{ \begin{array}{l} \cdots + \left[\frac{\Delta F_y}{\Delta \alpha} (D_{cp} - D_{cg}) - \frac{\Delta D_{tether}}{\Delta \alpha} T_{tether} \cos\beta \right] (\cos\alpha - \Delta\alpha \sin\alpha) + \cdots \\ \cdots + \left[\frac{\Delta F_x}{\Delta \alpha} (D_{cp} - D_{cg}) - \frac{\Delta D_{tether}}{\Delta \alpha} T_{tether} \cos\beta \right] (\sin\alpha + \Delta\alpha \cos\alpha) \end{array} \right\} \frac{\partial M_{ccw,cg}^{before}}{\partial \alpha} + \cdots$$

Risk #1: $\cos\beta$

β is the angle between the vertical and the tether line where it is attached to the bridle. For normal flight, when the kite flies overhead but slightly downwind from the vertical, β will be a small positive angle. If the kite zooms upwind past the vertical, β can become negative. It does not matter. As long as the kite is above the horizon, β will be somewhere between $-89°$ and $+89°$, to be extreme about it, and $\cos\beta$ will be strictly positive.

Risk #2: $\cos\alpha - \Delta\alpha \sin\alpha$

This term is not a risk. A bit of through will show that it is strictly positive for any realistic flight condition. Practically speaking, the angle of attack will always be between $0°$ and $30°$. The value of $\cos\alpha$ exceeds the value of $\sin\alpha$ all across that range. Since $\sin\alpha$ is further reduced by the factor $\Delta\alpha$, which is itself very small, the danger it poses is reduced even further. In short, $\cos\alpha - \Delta\alpha \sin\alpha$ is strictly positive.

Risk #3: $\sin\alpha + \Delta\alpha \cos\alpha$

For realistic flight conditions, where $0° < \alpha < 30°$, both $\sin\alpha$ and $\cos\alpha$ are positive. When the perturbation is nose-up, in the direction which increases the angle of attack and corresponds to $\Delta\alpha > 0$, the term is strictly positive. There is no risk from nose-up perturbations.

For nose-down perturbations, $\Delta\alpha < 0$, and the term could potentially go negative. The risk increases the smaller the angle of attack. Mathematically, the term will be algebraically negative if:

$$\sin\alpha + \Delta\alpha \cos\alpha < 0$$
$$\rightarrow \quad \Delta\alpha < -\frac{\sin\alpha}{\cos\alpha}$$
$$\rightarrow \quad \Delta\alpha < -\tan\alpha \qquad (17)$$

For small angles of attack α, we can invoke the small angle approximation for the tangent function, that $\tan\alpha \cong \alpha$. Equation (17) then reduces to $\Delta\alpha < -\alpha$. This has physical meaning. It means that the nose-down perturbation is greater than the angle of attack. In a way, this is obvious. If the nose-down perturbation is greater than the angle of attack, then the kite will have a negative angle of attack. Its stability becomes less important in the face of the emergency posed by the deflated surface.

From a practical point of view, then, we can treat this term as strictly positive, subject to the caveat that negative angles of attack may lead to a crash anyway.

Risk #4: $D_{cp} - D_{cg}$

This is the key risk, but one the designer or rigger can control. D_{cp} is the distance aft to the center-of-pressure from the leading edge. D_{cg} is the distance aft to the center-of-gravity from the leading edge. The difference $D_{cp} - D_{cg}$ is the distance by which the center-of-pressure lies aft of the center-of-gravity. So long as the center-of-gravity is kept forward of the center-of-pressure, this term will be strictly positive.

Since all of the terms on the right-hand side of Equation (16) are algebraically positive (a least near the equilibrum point chosen for this numerical example), the left-hand side will be algebraically positive as well. So, what is the left-hand side?

The left-hand side is another derivative expressed in terms of differences rather than differentials.

$$\frac{\Delta M_{ccw,cg}}{\Delta\alpha} = \frac{\text{Change in counter - clockwise moment}}{\text{Change in angle of attack}} > 0 \quad (18)$$

It is vital for this derivative to be algebraically positive.

- If the angle of attack increases ($\Delta\alpha > 0$), the counter-clockwise moment will increase ($\Delta M_{ccw,cg} > 0$). Counter-clockwise in the defining diagram was nose-down. The tendency of the kite after a nose-up perturbation is a nose-down moment.
- If the angle of attack decreases ($\Delta\alpha < 0$), the counter-clockwise moment will decrease ($\Delta M_{ccw,cg} < 0$). The tendency of the kite after a nose-down perturbation is a nose-up moment.

Both of these are restorative tendencies. They tend to rotate the kite back towards the equilibrium angle of attack following a perturbation. The tendency to restore the equilibrium is what makes an equilibrium stable.

This analysis is certainly not the final word on stability. We got lucky. At our selected equilibrium point, all of the terms made helpful contributions to stability. They were so helpful, in fact, that we did not have any need to delve into the next issue relating to stability, which is the location of the bridle attachment point. Since there were no negative terms in the principal stability derivative, we did not need to investigate which positive terms could be used to counter the negative ones. The bridle attachment point can be used for that purpose. Moving the attachment point effects the derivative $\Delta D_{tether}/\Delta\alpha$. That should be a topic for a later study.

Jim Hawley
September 2014

An e-mail describing errors or omissions would be appreciated.